SURFACE ELASTICITY MODELS FOR STATIC AND DYNAMIC RESPONSE OF NANOSCALE BEAMS

by

Chang Liu

B.Sc., Hunan University, P. R. China, 2007

A THESIS SUBMITTED IN PARTIAL FULLFILLMENT OF THE REQUIREMENTS FOR THE DEGREE OF

MASTER OF APPLIED SCIENCE

in

THE FACULTY OF GRADUATE STUDIES
(Mechanical Engineering)

THE UNIVERSITY OF BRITISH COLUMBIA
(Vancouver)

February 2010

Abstract

Nanoscale beam-like structures have attracted much attention due to their superior mechanical properties for applications in nanomechanical and nanoelectromechanical systems (NEMS). Nanoscale structures are characterized by a high surface to volume ratio. The elastic response of surface layers of atoms is different from that of the bulk atoms due to reduced connectivity. Thus, surface energy has a significant effect on the response of nanoscale structures, and is associated with their size-dependent behavior. The classical continuum mechanics fails to capture the surface energy effects and hence is not directly applicable at nanoscale. To overcome this limitation, modified continuum models incorporating surface energy effects need to be developed in order to evaluate the size-dependent mechanical response of nanoscale structures.

This thesis presents a modified continuum model and finite element formulation to study the static and dynamic response of nanoscale beams. The objective is to provide NEMS designers with an efficient set of tools that can predict static deflections, natural frequencies of vibrations, and uniaxial buckling loads of nanoscale beams with different geometries, applied forces, and boundary conditions. A general beam model based on Gurtin-Murdoch continuum surface elasticity theory is developed for the analysis of thin and thick beams of arbitrary cross-section. Closed-form analytical solutions for static bending of thin and thick beams under different loadings and boundary conditions are obtained. Their free vibration characteristics are also investigated. Analytical expressions for critical buckling loads of thin beam are presented. An intrinsic length scale depending on both surface and bulk elastic properties is defined to characterize surface energy effects in beam bending problems. The finite element simulation results of static bending, free vibration and axial buckling of nanoscale beams are compared with the analytical solutions for validation. Selected numerical results are presented for aluminum and silicon beams to demonstrate their salient response features. A technique is proposed to estimate surface elastic properties from measured natural frequencies of GaAs cantilever specimen. The surface elasticity continuum mechanics and finite element models developed in this work provide designers efficient tools to predict mechanical response of beam structures in nano devices.

Table of Contents

List of Tables

List of Figures

List of Symbols

A	Cross-sectional area of beam
b	Width of a beam with rectangular cross-section
D	Diameter of a beam with circular cross-section
E	Young’s modulus
F_{cr}	Modified critical buckling load of thin beam with surface effects
H	Height of a beam with arbitrary cross-section
$2h$	Height of a beam with rectangular cross-section
K_b	Modified bending stiffness of a thin beam with surface effects
K_s	Modified bending stiffness of a thick beam with surface effects
L	Length of beam
M^T	Moment resultant of thick beam
M^E	Moment resultant of thin beam
n	Wave number
$S_{\alpha\beta\gamma\delta}$	Surface elastic constant tensor
s^*	Perimeter moment of inertia
w	Vertical deflection of beam
ϕ	Angular displacement of beam cross-section
τ_0	Surface residual stress under unconstrained condition
λ_0 , μ_0	Surface Lamé constants or surface elastic constants
υ	Poisson’s ratio
ω	Natural frequency

Acknowledgements

I would like to express my heartfelt gratitude to my supervisors, Professor Nimal Rajapakse, and Dr. Srikantha Phani, whose patient guidance and continuous support enabled me to complete this thesis. I gratefully acknowledge the support from Professor Nimal Rajapakse's grant from the Natural Sciences and Engineering Research Council of Canada (NSERC).

Last but not least, I am indebted to my family, specially my parents, for their constant support and encouragement.

To my parents

Chapter 1

INTRODUCTION

1.1 Nanotechnology

Nanotechnology is an emerging technology involving the characterization, design, production and application of materials, structures and systems through the control of matter on the nanometer length scale, that is, at the level of atoms and molecules. A nanometer is one billionth of a meter ($10^{-9} m$). This is roughly four times the diameter of an individual atom. For comparison, a red blood cell is approximately 7,000nm wide and a water molecule is almost 0.3nm across. Materials and structures with at least one dimension in $1-100nm$ are within the purview of nanotechnology. In this realm, nanomaterials and nanostructures exhibit properties and phenomena that cannot be observed at macro-scale, which opens new prospects of technology innovation.

Nanotechnology is a multi-disciplinary field. In a famous speech entitled “There is plenty of room at the bottom” [1] Richard Feynman enunciated the key challenges to be addressed in small-scale systems in 1959. He predicted the ability to manipulate individual atoms and molecules to create new materials, structures and devices which would lead to revolutionary changes in all aspects of our life. He also pointed out that, for this to happen, a set of precise tools were needed to observe and operate such nanoscale objects. It was not until 1980s that the instruments such as scanning tunneling microscopes (STM) and atomic force microscopes (AFM) were invented, providing the researchers with efficient tools to manipulate the nanomaterials and detect their novel properties. Thereafter, many avenues of research in nanoscience and nanotechnology have opened. Over the past decade, nanomaterials and nanostructures have been synthesized and exploited in a wide range of applications, such as computers, medicine, advanced materials, communication, etc. With increasing demand for high performance devices and fast pace of miniaturization, nanotechnology will undoubtedly become central to the epoch of technology era and profoundly impact our industries and society.

Nanomaterials and nanostructures, such as nanolayers, nanowires, nanotubes and nanoparticles are the outcomes of direct molecular manipulation and also the fundamental building blocks for the nanocomposites, nanosystems and nanodevices. In this special length scale, quantum effects and surface effects become dominant, which lead to the fundamental change in material properties (for instance, mechanical, electrical, magnetic, optical, chemical and other properties), triggering ever-broader applications. For example, the nanoparticles and nanolayers have a high surface to volume ratio, making them ideal for applications in chemical reaction, combustion, composite materials and energy storage. Nanoparticles made of semiconducting material are used in biomedical applications as drug carriers or imaging agents. Carbon nanotubes (CNT) are reported to have Young's modulus five times that of steel (Young's modulus of CNT is in the range of 1.0 to 5.0 Tpa) [2, 3], a hundred times of its tensile strength and only one-sixth of its weight. Meanwhile the electrical conductivity is six orders of magnitude higher than copper. As a result, they are used in nanocomposite fibers, field emission panel displays, chemical sensing, nanoelectronics, etc. Nanoporous membranes with pores smaller than 10 nm are suitable for novel mechanical filtration devices. Nanowires are being explored to make efficient solar cells due to their unique chemical and electrical properties. Dispersions of conducing nanowires in different polymers are being investigated for use as transparent electrodes for flexible flat-screen displays. It is apparent that the unique properties and phenomena observed at nanoscale will provide significant enhancement beyond what current technologies have established. A comprehensive introduction of nanotechnology and current breakthroughs can be found in a recent report [4].

1.2 Nanomechanics

To successfully design and manufacture the nanostructured materials, devices and systems, a fundamental understanding of their mechanical behavior is required. Nanomechanics is a new area of mechanics concerned with the study of mechanical properties and response of materials and structures at the nanoscale. In this regard, experimental techniques, theoretical models and computational tools are being developed to investigate the mechanics of nanomaterials and nanostructures, such as their effective elastic moduli, bending stiffness, buckling loads, and tensile/compressive strengths.

Experimental developments have brought about striking progress in nanotechnology in the last few decades. The development of advanced instrumentation tools enables the researchers to resolve and characterize objects at nanoscale level. Among the various techniques, scanning probe microscopy has been a major tool in investigating the properties of individual nanostructures. For example, Tomasetti et al. [5] quantitatively assessed the elastic modulus of polymers and polypropylene by measuring their indentation hardness with an atomic force microscope (AFM). Cuenot et al. [6] measured the elastic modulus of metallic nanowires and polymer nanotubes with varied diameter using a resonant-contact AFM. Wong et al. [7] used AFM to measure the mechanical properties of individual, structurally isolated silicon carbide nanorods and multiwall carbon nanotubes that were pinned at one end to molybdenum disulfide surfaces. Han et al. [8] developed an *in situ* transmission electron microscopy method for conducting bending or axial tensile experiments for nanowires and nanotubes in transmission electron microscopy. The experimental results can provide verifications for the theoretical and numerical modeling. A continuous development of advanced experimental equipment and methodology is required for further development of nanoscience and nanotechnology.

Another approach is atomistic simulation which deals with the motion of atoms and characterizes the behavior of the nanoscale objects by considering a cluster of atoms. The two main molecular simulation methods are *ab initio* quantum mechanical methods and molecular dynamics (MD). The *ab initio* methods are based on the first principles and deal with the solutions to the Schrödinger equation [9]. In general, *ab initio* methods give more accurate results than MD, but they are also much more computationally intensive. MD is widely used in atomistic modeling. It looks at the interactions of atoms or molecules for a period of time and the objective is to solve the governing equations of particle dynamics based on Newton’s second law. As the atomistic simulations reflect the real configurations of the structures, the results obtained from this approach can be very accurate. However, in engineering applications where the materials and structures are normally modeled up to a scale of several microns, consisting billions of atoms, the atomistic simulations have difficulty in analyzing such structures due to the computational limitations in length and time scales.

In searching for more efficient ways to model practical nanoscale systems, many researchers have resorted to the continuum mechanics approaches due to their superior computational efficiency and versatility. However, the conventional continuum mechanics is based on the assumption that quantities vary slowly over atomic length scale; it fails to capture the atomic features of the nanostructures. To overcome this limitation, a set of modified continuum theories has been proposed to incorporate the quantum/molecular effects existing at the nanoscale into the conventional continuum framework. The main approach is to incorporate some special parameters extracted from interatomic potentials or atomistic properties into the continuum mechanics model. Several such models have been successfully developed, such as multi-scale continuum models, surface elasticity models and non-local elasticity models. They have shown good agreement with atomistic simulations, and surpass the atomistic models in terms of computational efficiency and versatility.

1.3 Review of Surface Elasticity Model

One significant reason that gives rise to the exceptional properties and behaviour of nanomaterials and nanostructures is the surface energy. As explained by Streitz et al. [10], the atoms at a free surface or interface are exposed to a different environment than those in the bulk of a material; the equilibrium position and energy of those atoms are consequently different from bulk positions and energies. Properties of the solid which are sensitive to the atomic positions or energies are necessarily affected at or near a surface or interface. Especially for thin films or layered structures where there are a great number of atoms near the surface or interface compared to that in bulk, these surface effects can be substantial.

The surface energy quantity referred to as the surface free energy or excess surface energy γ was first introduced by Gibbs [11] in the thermodynamics of solid surfaces. It is equal to the reversible work per unit area needed to create a surface by a process such as cleavage or creep. The ratio of surface free energy $\gamma (J / m^2)$ to Young's modulus

$E\ (J/m^3), \gamma/E$, is dimensional (m) and points to some other intrinsic length scale parameter of a material [12]. This intrinsic length scale is usually small, in the nanometer range or even smaller. When a material element has one characteristic length comparable to the intrinsic scale, the surface/interface free energy can play an important role in its properties and behaviour. There is another fundamental parameter, called surface stress, which was also defined by Gibbs [11] for the first time. It is associated with the reversible work per unit area needed to elastically stretch a pre-existing surface. The relationship between the surface stress and surface free energy has been formulated as [13, 14]

$$\sigma_{\alpha\beta} = \gamma\delta_{\alpha\beta} + \partial\gamma/\partial\varepsilon_{\alpha\beta} \tag{1.1}$$

where $\sigma_{\alpha\beta}$ and $\varepsilon_{\alpha\beta}$ denote the surface stress and strain, respectively, and $\delta_{\alpha\beta}$ is the Kronecker delta, $\delta_{\alpha\beta} = \begin{cases} 1 & \alpha = \beta \\ 0 & \alpha \neq \beta \end{cases}$. Note that the surface free energy γ is a scalar, while the surface stress $\sigma_{\alpha\beta}$ is a second rank tensor in tangent plane of the surface and the strain normal to surface is excluded in Eq. (1.1) and α and β take integers 1 or 2. The form of Eq. (1.1) is shown to depend on the coordinate frame of reference. In the Eulerian frame of reference where the surface/interface area changes with strain, surface/interface stress is in the expression of Eq. (1.1). However, in Lagrangian coordinates embedded in elastically deforming material, the surface/interface stress appears explicitly as a variation of surface/interface free energy with elastic strain [15].

By analogy to constitutive relationship for bulk material in elasticity, Miller and Shenoy [16] suggested a linear surface constitutive equation by introducing a set of surface elastic constants as,

$$\sigma_{\alpha\beta} = \tau^0_{\alpha\beta} + S_{\alpha\beta\gamma\delta}\varepsilon_{\gamma\delta} \tag{1.2}$$

where $\tau^0_{\alpha\beta}$ is the surface stress when the bulk is unstrained, and $S_{\alpha\beta\gamma\delta}$ is the fourth order surface elasticity tensor. Due to the symmetries, there are a total of nine independent elastic constants for a crystal surface. The number of independent elastic constants can be further reduced according to the surface geometric symmetry [17].

Gurtin and Murdoch [18, 19] proposed a generic theoretical framework based on continuum mechanics concepts that accounts for the surface/interface energy. In their model, the surface is regarded as a mathematical layer of zero thickness adhered to the underlying bulk material without slipping. The surface properties are different from those in the bulk and are characterized by the surface residual stress and surface Lamé constants. For an isotropic surface, the surface stresses and strains are related by the following surface constitutive equation.

$$\sigma_{\alpha\beta} = \tau^0\delta_{\alpha\beta} + (\lambda^S + \tau^0)\varepsilon_{\gamma\gamma}\delta_{\alpha\beta} + 2(\mu^S - \tau^0)\varepsilon_{\alpha\beta} \tag{1.3}$$

where τ^0 is the surface residual stress without constraint; λ^S and μ^S are surface Lamé constants or surface elastic constants.

The above mathematical formulation suggests that the elastic responses of nanostructures significantly depend on the surface elastic constants, which could be determined by experiments or atomistic simulations. Vermaak et al. [20, 21] determined the absolute surface stresses by observing the contraction of small gold, silver and platinum particles under the influence of the surface stress. Their experimental results for surface stress are 1.175, 1.415 and 2.574 N/m respectively. Jing et al. [22] measured the elastic properties of silver nanowires by using contact AFM. A good review of experimental work can be found in [23, 24]. Besides the experiment efforts, many theoretical approaches have been used to predict the surface properties. Surface stresses were evaluated using *ab initio* methods in semiconductors by Maede et al. [25] and in metals by Needs [26].With the assumption of isotropy, Miller and Shenoy [16] computed surface moduli of different surface orientations by using the embedded atom method (EAM) for FCC Al and Stillinger-Weber empirical potentials for Si. Dingreville et al. [27, 28] used a semi-analytic method to compute the surface elastic properties of crystalline materials. A systematic study of surface elastic constants using atomistic simulations has been presented by Shenoy [17]. The surface elastic parameters of several crystal faces of FCC crystal metals were computed. From their simulations, it is found that the surface elastic tensor $S_{\alpha\beta\gamma\delta}$ need not be positive definite, i.e., the quadratic form $S_{\alpha\beta\gamma\delta}\varepsilon_{\alpha\beta}\varepsilon_{\gamma\delta}$ can be negative, which may suggest a violation of basic thermodynamic postulates. To explain this phenomenon, Shenoy pointed out that the positive definiteness of the bulk elastic modulus tensor which guarantees the solid stability can not be applied to the surface elastic tensor. Though it is treated separately in the study, the surface can not exist independently without the bulk and the total energy (bulk+surface) still satisfies the positive definite condition.

According to the generalized Young-Laplace equation, the presence of surface stresses gives rise to a set of non-classical boundary conditions. These non-classical boundary conditions and surface stress-strain relations, along with the classical elasticity equations for the bulk form a coupled system of field equations. Gurtin and Murdoch's model [18, 19] has been widely adopted to investigate a variety of size-dependent problems at nanoscale. For instance, Hamilton and Wolfer [29] presented an embedded atom method calculation of the surface elastic constants of Cu (111) using the Gurtin and Murdoch theory. Miller and Shenoy [16] and Shenoy [30] developed a one-dimensional model to demonstrate that the surface effects can be modeled as additional terms to the overall elastic moduli of structural elements in uniaxial tension, bending and torsion and the results are generally in a good agreement with the atomistic simulations. Wang et al. [31] investigated the influence of surface tension and the residual stress field in the bulk induced by surface tension on the elastic deformation of nanostructures. Sharma and Ganti [32] and Sharma [33] studied the size-dependent strain states of inhomogeneities and Eshelby tensor for nanoinclusions with surface energy. Tian and Rajapakse [34] investigated a cylindrical nanoinclusion under a two-dimensional dilatational eigenstrain and far-field loading. Wang and Feng [35] extended the surface elastic model to study the effects of surface stresses on contact problems and derived the closed-form solution of the deformation around an elliptic hole including the surface energy effects. Zhao and Rajapakse [36] examined the plane and axisymmetric problems for a surface-loaded elastic layer in the presence of surface energy effects.

1.4 Nanoelectromechanical Systems

An important area of nanotechnology that has received increasing interests in recent years is the design and fabrication of nanomechanical and nanoelectromechanical systems (NEMS). These are devices integrating electrical and mechanical functionality at nanoscale. In this regime, NEMS offer a number of unique attributes such as small size, low mass, high mechanical resonance frequencies, and high sensitivity. Application of NEMS includes actuators, sensors, machines and electronics at nanoscales [37]. NEMS can be used to measure extremely small displacements and forces that lead to new developments for applications in medicine, computers, communications, etc. The principal components of NEMS are mechanical elements that either deflect or vibrate in response to the external excitations, and a transducer that can convert mechanical energy to electrical or optical signals. Nanostructures such as nanobeams, nanoplates and nanomembranes are the common components of NEMS mechanical parts. Structural integrity, reliability and durability of NEMS are important issues in practical applications. Therefore, understanding the mechanical properties, response and stability of NEMS structural elements is crucial to the exploitation of NEMS technology.

Due to the surface energy effects at nanoscale, the investigation of the mechanical behavior of nanostructures with surface energy effects remains a topic of substantial interest. Lagowski et al. [38] carried out an experiment to measure the natural frequencies of GaAs wafers in the configuration of cantilever beams within a small scale region. They found that the natural frequencies substantially depend on the surface stress which cannot be explained by classical theory of vibration. To investigate this experimental phenomenon, Gurtin et al. [39] developed a simple one-dimensional beam model to illustrate that the beam resonant frequency is independent of the surface stress and therefore the experimental results require a different explanation. Wang and Feng [40] developed a sandwich-beam model to study the effects of surface elasticity and surface tension on the natural frequencies of micro- or nanosized beams and revealed that when the thickness of beams reduces to microns or nanometers, both the surface elasticity and surface tension have significant effects on its vibration frequency. Yang et al. [41] and Ekinci and Roukes [42] have fabricated nanometer scale electromechanical beam resonators and examined their response experimentally. Wang et al. [43] studied the surface buckling of a microbeam due to surface energy effects. Sadeghian et al. [44] studied the effects of surface stress on resonance frequency of nanocantilevers. Recently, Lachut and Sader [45] proposed a three-dimensional model to examine the surface stress effects on the stiffness of cantilever plates. Lim and He [46] analyzed the deformations of nanofilms under bending by incorporating the surface elasticity effects into Von

Karman plate theory. Lu et al. [47] complemented Lim and He's model [48] by considering the normal stress variation along the thickness direction and presented a general model for static and dynamic analysis of thin film structures. He and Lilley [49, 50] studied the surface energy effects on static bending and bending resonance of nanowires with different boundary conditions.

1.5 Scope of the Current Work

Based on the above introduction and literature survey, it can be seen that understanding the size-dependent behavior of beam-like structures at nanoscale is essential for effective NEMS design. The continuum modeling approach accounting for surface energy effects is considered to be attractive due to its simplicity and computational efficiency. Current continuum models available for studying the beam response with surface effects are confined to beams with simple geometries and boundary conditions. Meanwhile these models are mostly developed to analyze thin beams (Euler beams), which fail to capture the shear deformations that are important when the aspect ratio becomes relatively small (In the present context, aspect ratio corresponds to height-to-length ratio) and also for the analysis of higher natural frequencies. The aim of this thesis is to develop a general beam model based on Gurtin-Murdoch theory to analyze thin and thick nanoscale beams with an arbitrary cross-section. The model is further applied to investigate the static bending, uniaxial buckling and free vibration of such beams respectively. A finite element scheme is also presented to analyze the nanoscale beam structures with complex geometries and boundary conditions. This thesis has two main objectives: first, to show the significance of surface effects on the beam static and dynamic response and structural stability; second, to provide a set of analytical solutions and numerical tools to the designers in NEMS and other nanoscale devices.

Chapter 2 presents the detailed formulation of the governing equations of a beam including surface energy effects. Surface pre-stress as well as surface elasticity are considered. Based on the general model, thin beam (Euler-Bernoulli beam) and thick beam (Timoshenko beam) theories accounting for surface effects are established. Analytical solutions for static response of thin and thick beams under different loading (point and uniformly distributed loading) and boundary conditions (simply-supported, cantilever and both ends clamped) are derived. The stability of beam structures under axial compression is also investigated and the critical loads for different beam restraints are presented. To the best of our knowledge, such solutions have not been reported previously. The numerical results of deflection profiles and critical loads of selected beams based on the proposed models are also presented, and compared with the solutions from classical thin and thick beam theory to quantitatively assess the influence of surface energy effects.

Chapter 3 studies the dynamic response of thin and thick beams. Analytical solutions of free vibration characteristics of such beams are derived. The numerical results of natural frequency and mode shape of selected beams are presented and again compared with the classical solutions to examine the surface energy effects. The energy approach, Rayleigh quotient, is also applied to derive the closed-form solution of natural frequencies for thin beams. The solutions are further employed to fit the experimentally measured natural frequencies of GaAs cantilever beams reported in [38]. A suggestion for the determination of surface stress and surface elastic constants by measuring the natural frequency of free vibration is thereafter proposed.

In Chapter 4, a finite element scheme is developed to study the complex beam problems encountered in NEMS and other nanotechnology applications. In conventional finite element method (FEM) surface elasticity effects are not considered. Therefore, new thin and thick beam elements considering surface effects are developed respectively. The finite element formulation based on Galerkin's method is first presented and then verified by simulating the static deflections, natural frequencies and buckling problems of selected beams and comparing the results with the analytical solutions obtained from Chapter 2 and 3.

Chapter 5 concludes the major findings of the thesis, summarizes the contributions of current study and provides suggestions for future work.

Chapter 2

STATIC AND DYNAMIC ANALYSIS OF NANOSCALE BEAMS

2.1 Problem Description

Based on the previously reported work, the surface elasticity theory is extended in this section to study the size-dependent behavior of nanoscale beams. A general mechanistic model based on Gurtin-Murdoch continuum theory accounting for surface effects is presented. Thereafter the thick and thin beam models incorporating surface elasticity effects are developed in order to analyze the static and dynamic response of nanoscale beams. The thin beam model is based on Euler-Bernoulli beam theory, in which the shear deformations are neglected and plane sections remain normal to the neutral axis after bending. It gives good results for slender beams where bending dominates the deformation fields. The thick beam model is based on Timoshenko beam theory. The shear deformation is taken into account; consequently, the assumption of plane sections to remain plane after deformation is relaxed. It is suitable for analyzing short and stocky beams where the shear effects are significant.

A nanoscale beam with length L and height H is modeled in Cartesian coordinate system (x, y, z) as shown in Figure 2.1. The cross-section is arbitrary (symmetric about z-axis) with unit normal n and tangent t. The area and perimeter of the cross-section are A and s respectively. To incorporate the surface effects, it is assumed that the response of the beam is governed by the continuum theory proposed by Gurtin and Murdoch [18, 19]. Unlike the classical case, the beam in Gurtin-Murdoch model has an elastic surface with zero thickness fully bonded to its bulk material. Bulk materials are assumed to be homogeneous and isotropic with Young's modulus E, Poisson's ratio v and mass density ρ. The stress state of the bulk material of the beam is assumed to be plane stress with the non-zero stresses, σ_{xx}, σ_{xz} and σ_{zz} as shown in Figure 2.2. The corresponding bulk strains are ε_{xx}, ε_{xz} and ε_{zz}. The equilibrium and constitutive equations for the bulk solid are the same as those in classical elasticity theory [52]. In general, the elastic surface (outward unit normal n and unit tangent t) has surface stress components τ_{xx}, τ_{tx}

and τ_{nx} shown in Figure 2.2. In the engineering beam theory, only τ_{xx} and τ_{nx} are considered. The elastic properties of surface materials are Lamé constants λ_0, μ_0 and surface residual stress under unstrained conditions τ_0, and the mass density of the surface is ρ_0.

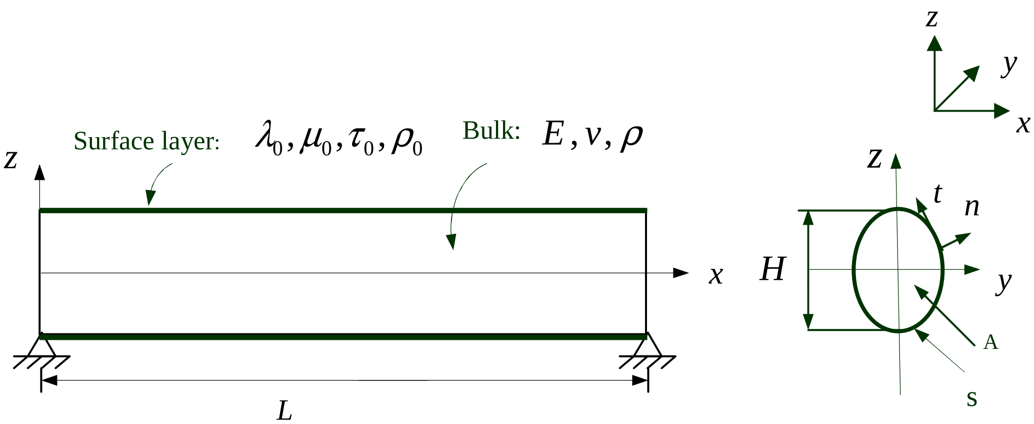

Figure 2.1 Geometry of beam with arbitrary cross-section and coordinate system

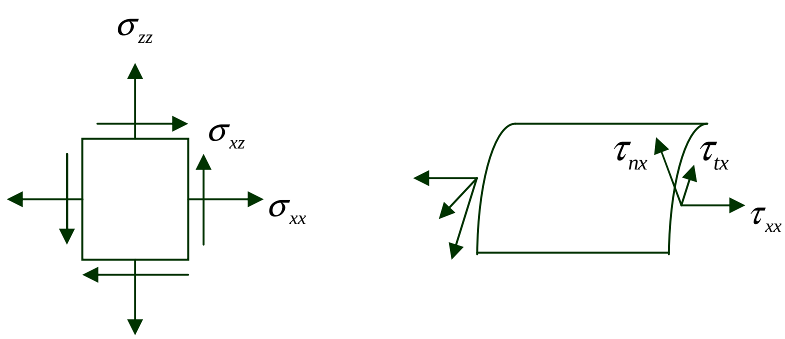

Figure 2.2 State of stress of the bulk and surface

2.2 Formulation of General Beam Surface Elasticity Model

Consider a free-body diagram for a small segment Δx of the beam (bulk) as shown in Figure 2.3. The internal resultant shear force Q and moment M act on both faces of the segment. On the right hand face, there are infinitesimal increments in Q and M respectively**.** The inertia forces $\rho\ddot{u}_x$ and $\rho\ddot{u}_z$ exist in the segment body. For the purpose of generality, the beam is subjected to an arbitrary lateral loading $q(x)$ along the beam length. As a result of the interaction between the elastic surface and bulk materials, the traction $T_i = \sigma_{ij} n_j$ act on the overall surface of the bulk element (In the free-body diagram, only the tractions on the top surface of the bulk are shown). Within the beam, plane stress state implies non-zero tractions T_x and T_z only. Note that the out-of-plane stress T_z is induced from the in-plane stresses when the beam is deformed due to the generalized Young-Laplace equation.

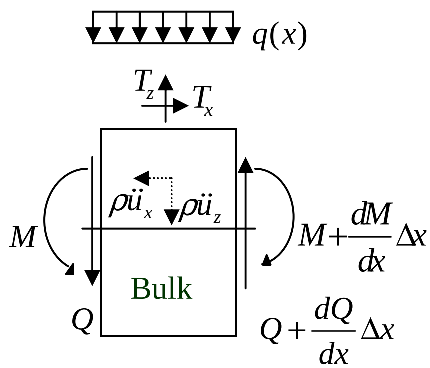

Figure 2.3 Free-body diagram of a segment of the beam

The vertical force and moment equilibrium equations of the bulk element can be written as:

$$\frac{dQ}{dx} + \int_s T_z ds - q(x) - \int_A \rho \ddot{u}_z dA = 0 \quad (2.1)$$

$$\frac{dM}{dx} + \int_s T_x z ds - Q - \int_A \rho \ddot{u}_x z dA = 0 \quad (2.2)$$

where the shear force resultant and bending moment resultant are defined as, $Q = \int_A \sigma_{xz} dA$ and $M = \int_A \sigma_{xx} z dA$, respectively.

The equilibrium relations for the surface can be expressed in terms of the surface and bulk stress components as [18, 19],

$$\tau_{i\alpha,\alpha} - T_i = \rho_0 \ddot{u}_i^s \quad (2.3)$$

Where $i = x, n, t$ and $\alpha = x, t$; τ denotes the surface stress. $\ddot{u}_i^s$ denotes the acceleration of surface layer in the i direction. The presence of surface stress and inertia results in the surface traction. Rewriting the non-zero surface tractions T_x and T_z in form of surface stress and inertia terms from equation (2.3) yields the following,

$$T_x = \tau_{xx,x} - \rho_0 \ddot{u}_x^s \tag{2.4}$$

$$T_z = T_n n_z = (\tau_{nx,x} - \rho_0 \ddot{u}_n^s) n_z \tag{2.5}$$

where $n_z = \cos < n, z >$ is the direction vector.

Substitution of equations (2.4) and (2.5) into (2.1) and (2.2) yields the following equilibrium equations,

$$\frac{dQ}{dx} + \int_s \tau_{nx,x} n_z ds - q(x) = \int_A \rho \ddot{u}_z dA + \int_s \rho_0 \ddot{u}_n^s n_z ds \tag{2.6}$$

$$\frac{dM}{dx} + \int_s \tau_{xx,x} z ds - Q = \int_A \rho \ddot{u}_x z dA + \int_s \rho_0 \ddot{u}_x^s z ds \tag{2.7}$$

Note that in the absence of the surface stresses and inertia, equation (2.6) and (2.7) are reduced to the classical beam bending moment and shear force relationships.

Since both the bulk and surfaces of the beam are assumed to be homogeneous and isotropic, the constitutive relations of the bulk material relating non-zero stresses σ_{xx}, σ_{xz} and σ_{zz} to the corresponding strains can be expressed as,

$$\begin{aligned} \sigma_{xx} &= E\varepsilon_{xx} + \nu\sigma_{zz} \\ \sigma_{xz} &= 2G\varepsilon_{xz} \end{aligned} \tag{2.8}$$

where E is the elastic modulus, ν is Poisson's ratio and G is the shear modulus.

Note that in a beam bending problem, the stress component σ_{zz} is not zero. But it is small enough compared to axial stress σ_{xx} to neglect in classical beam theory. However, in Gurtin-Murdoch model the surface is not in balance with the above assumption. To remedy this, following Lu et al. [47] σ_{zz} is assumed to vary linearly through the beam thickness and satisfy the equilibrium conditions on the surface. The significance of σ_{zz} on the beam responses will be further investigated in the following section while presenting numerical results. With this assumption, σ_{zz} can be written as,

$$\sigma_{zz} = \frac{1}{2}(\sigma_{zz}^+ + \sigma_{zz}^-) + \frac{z}{H}(\sigma_{zz}^+ - \sigma_{zz}^-) \tag{2.9}$$

where the superscripts + and − denote the surface quantities on the very top and bottom points of the surface layer respectively. σ_{zz}^{+} and σ_{zz}^{-} are stresses at the top and bottom fibers respectively where the outward unit normal vector n is parallel to the z direction, and H is the height of the beam.

Rewriting σ_{zz} in terms of surface stresses and inertia yields,

$$\sigma_{zz} = \frac{1}{2}(\tau_{zx,x}^{+} + \tau_{zx,x}^{-} - \rho_0 \ddot{u}_z^{+} - \rho_0 \ddot{u}_z^{-}) + \frac{z}{H}(\tau_{zx,x}^{+} - \tau_{zx,x}^{-} - \rho_0 \ddot{u}_z^{+} + \rho_0 \ddot{u}_z^{-}) \tag{2.10}$$

The surface constitutive relations given by Gurtin and Murdoch [18, 19] can be simplified in present study as,

$$\tau_{xx} = \tau_0 + (2\mu_0 + \lambda_0) u_{x,x}$$

$$\tau_{nx} = \tau_0 u_{n,x} \tag{2.11}$$

where τ_0 is the residual surface stress under unconstrained conditions; μ_0 and λ_0 are surface Lamé constants.

2.2.1 Thick Beam Surface Elasticity Model

In the thick beam model where the shear deformation and rotational inertia effects are considered (Timoshenko beam theory), the cross-sectional rotation is an independent variable in addition to the transverse (vertical) deflection of the neutral axis. Therefore the displacement field is given as [52],

$$u_x = z\phi(x,t)$$

$$u_z = w(x,t) \tag{2.12}$$

where $\phi(x,t)$ and $w(x,t)$ are the angular displacement and transverse displacement of beam respectively.

The state of non-zero strains are expressed in the strain-displacement relations as,

$$\varepsilon_{xx} = \frac{\partial u_x}{\partial x} = z\frac{\partial \phi(x,t)}{\partial x}$$

$$\varepsilon_{zz} = 0$$

$$\varepsilon_{xz} = \frac{1}{2}\left(\frac{\partial u_x}{\partial z} + \frac{\partial u_z}{\partial x}\right) = \frac{1}{2}\left(\frac{\partial w(x,t)}{\partial x} + \phi(x,t)\right) \tag{2.13}$$

Substitution of equation (2.12) into equation (2.11) yields the following surface stress field,

$$\tau_{xx} = \tau_0 + z(2\mu_0 + \lambda_0)\frac{\partial \phi}{\partial x}$$

$$\tau_{nx} = \tau_0 \frac{\partial w}{\partial x} n_z \tag{2.14}$$

Therefore, the surface vertical stresses at the top and bottom of the surface layer can be obtained from equation (2.14) when $n_z = 1$,

$$\tau_{zx}^{+} = \tau_0 \frac{\partial w}{\partial x}$$

$$\tau_{zx}^{-} = -\tau_0 \frac{\partial w}{\partial x} \tag{2.15}$$

Substitution of equations (2.15) and (2.12) into equation (2.10), the vertical stress σ_{zz} can be derived as,

$$\sigma_{zz} = \frac{2z}{H}(\tau_0 \frac{\partial^2 w}{\partial x^2} - \rho_0 \ddot{w}) \tag{2.16}$$

Using equation (2.8), the non-zero bulk stresses can be written in the following form:

$$\sigma_{xx} = E(z\frac{\partial \phi}{\partial x}) + \frac{2\nu z}{H}(\tau_0 \frac{\partial^2 w}{\partial x^2} - \rho_0 \ddot{w})$$

$$\sigma_{xz} = G\kappa(\frac{\partial w}{\partial x} + \phi)$$

$$\sigma_{zz} = \frac{2z}{H}(\tau_0 \frac{\partial^2 w}{\partial x^2} - \rho_0 \ddot{w}) \tag{2.17}$$

where κ is the shear correction coefficient which accounts for the deviation from assumed constant shear stress along thickness direction in the Timoshenko beam theory. The values of κ for various cross-sectional shapes are given in standard texts such as Gere and Timoshenko [52].

Equation (2.17) and equation (2.14) give the stress field of the thick beam. By substituting both of the equations along with the displacement field in equation (2.12) into the general beam equilibrium equations (2.6) and (2.7), the governing equations for a thick beam including surface effects can be obtained as,

$$G\kappa A(\frac{\partial^2 w}{\partial x^2} + \frac{\partial \phi}{\partial x}) + \tau_0 s^* \frac{\partial^2 w}{\partial x^2} - q(x) = (\rho A + \rho_0 s^*)\frac{\partial^2 w}{\partial t^2} \tag{2.18}$$

$$[EI+(2\mu_0+\lambda_0)I^*]\frac{\partial^2\phi}{\partial x^2}+\frac{2\nu I\tau_0}{H}\frac{\partial^3 w}{\partial x^3}-G\kappa A(\frac{\partial w}{\partial x}+\phi)$$

$$=(\rho I+\rho_0 I^*)\frac{\partial^2\phi}{\partial t^2}+\frac{2\nu I\rho_0}{H}\frac{\partial^3 w}{\partial x\partial t^2} \tag{2.19}$$

where $I=\int_A z^2 dA$ is the moment of inertia of the beam cross-sectional area. $I^*=\int_s z^2 ds$ is the perimeter moment of inertia, an analogue to the moment of inertia for the bulk, and has units of [length^3]. $s^*=\int_s n_z^2 ds$ has the unit of length. All the above three parameters are dependent on the geometry of the cross-section. In the case of beams with a rectangular cross section of height $2h$ and width b, and a circular cross-section of diameter D, the parameters are given by,

$$H=\begin{cases}2h\\ D\end{cases},\ s^*=\begin{cases}2b\\ \pi D/2\end{cases},\ I=\begin{cases}2bh^3/3\\ \pi D^4/64\end{cases},\ I^*=\begin{cases}2bh^2+4h^3/3\\ \pi D^3/8\end{cases} \tag{2.20}$$

The resultant shear force and bending moment of beam cross section including the surface contributions can be expressed as,

$$\begin{aligned}Q^T&=G\kappa A(\frac{\partial w}{\partial x}+\phi)+\tau_0 s^*\frac{\partial w}{\partial x}\\ M^T&=[EI+I^*(2\mu_0+\lambda_0)I^*]\frac{\partial\phi}{\partial x}+\frac{2\nu I\tau_0}{H}\frac{\partial^2 w}{\partial x^2}-\frac{2\nu I\rho_0}{H}\ddot{w}\end{aligned} \tag{2.21}$$

where the superscript T denotes quantities belonging to thick beam model. Compared to the classical Timoshenko beam theory, in equation (2.18) the surface residual stress τ_0 introduce an additional second derivative term of the transverse deflection, and the inertia term on the right hand side of the equation is also modified by the surface mass density. In equation (2.19), it is found that the bending stiffness of the beam is modified due to the surface elastic constants; meanwhile the surface residual stress and surface mass density also come to influence by bringing the second terms on the left and right hand sides respectively. If the surface effects are completely neglected, namely λ_0, μ_0, τ_0 and ρ_0 are zero, equations (2.18) and (2.19) reduce to the governing equations of classical Timoshenko beam theory [52].

2.2.2 Thin Beam Surface Elasticity Model

The thin beam model (Euler-Bernoulli beam theory) is a more restricted case based on thick beam model with further simplified assumptions. It is normally applicable for the slender beams with span-to-thickness ratio $L/H \geq 20$ where the effects of shear deformation are small. Meanwhile the rotational inertia are also ignored, i.e. $\ddot{\phi} = 0$. Based on the above assumptions, equation (2.19) can be rewritten as,

$$G\kappa A(\frac{\partial w}{\partial x} + \phi) = [EI + (2\mu_0 + \lambda_0)I^*]\frac{\partial^2 \phi}{\partial x^2} + \frac{2\nu I\tau_0}{H}\frac{\partial^3 w}{\partial x^3} - \frac{2\nu I\rho_0}{H}\frac{\partial^3 w}{\partial x \partial t^2} \qquad (2.22)$$

Taking the first derivative of equation (2.22) with respect to x and substituting it into equation (2.18), together with the displacement assumption $\phi = -\frac{\partial w}{\partial x}$, the governing equation of thin beam model in the presence of surface effects can be obtained in terms of the transverse deflection as,

$$[EI + (2\mu_0 + \lambda_0)I^* - \frac{2\nu I\tau_0}{H}]\frac{\partial^4 w}{\partial x^4} - \tau_0 s^* \frac{\partial^2 w}{\partial x^2} + q(x)$$

$$= -(\rho A + \rho_0 s^*)\frac{\partial^2 w}{\partial t^2} - \frac{2\nu I\rho_0}{H}\frac{\partial^4 w}{\partial x^2 \partial t^2} \qquad (2.23)$$

The resultant shear force and bending moment are given by,

$$\begin{aligned} M^E &= -[EI + (2\mu_0 + \lambda_0)I^* - \frac{2\nu I\tau_0}{H}]\frac{\partial^2 w}{\partial x^2} - \frac{2\nu I\rho_0}{H}\ddot{w} \\ Q^E &= -[EI + (2\mu_0 + \lambda_0)I^* - \frac{2\nu I\tau_0}{H}]\frac{\partial^3 w}{\partial x^3} + \tau_0 s^* \frac{\partial w}{\partial x} - \frac{2\nu I\rho_0}{H}\frac{\partial \ddot{w}}{\partial x} \end{aligned} \qquad (2.24)$$

where subscript E denotes quantities belonging to thin beam model. Based on equation (2.23), the modified bending stiffness of a thin beam including surface effects can be defined as,

$$K_b = [EI + (2\mu_0 + \lambda_0)I^* - \frac{2\nu I\tau_0}{H}] \qquad (2.25)$$

Note that the surface residual stress (τ_0) contributes to the bending stiffness only due to the consideration of σ_{zz} in the formulation. If σ_{zz} is neglected then the last term in K_b containing τ_0 and the last inertial term on the right hand side of equation (2.23) vanish. Again if the surface effects are neglected (λ_0 , μ_0 , τ_0 and ρ_0 are zero), the governing equation (2.23) is identical to that in classical Euler-Bernoulli beam theory.

The ratio of change of bending stiffness due to surface effects to the classical bending stiffness is defined as,

$$\frac{K_b - EI}{EI} = \frac{[(2\mu_0 + \lambda_0) - 2\nu\tau_0 / \alpha]}{E} \frac{\alpha}{H} = \alpha \frac{H_0}{H} \tag{2.26}$$

where $\alpha = I^* H / I$ is a non-dimensional constant that depends on the geometry of the beam cross section. For example, α is calculated to be 8 for both square and circular cross sections. The first term of the length-scale is identical to Miller and Shenoy's analytical result for a nanobeam with a rectangular cross-section [16]. The second term is due to the consideration of surface residual stress which is not included in Miller and Shenoy's work. Zhu et al. [53] have investigated the combined effects of surface elasticity and surface residual stress on the bending stiffness. Their observations on the influence of surface residual stress are in agreement with our models. $H_0 = [(2\mu_0 + \lambda_0) - 2\nu\tau_0 / \alpha] / E$ is an intrinsic length parameter for the beam bending problem that sets a range in which the surface effects become significant. Note that E is a positive quantity, but the surface elastic constants and surface residual stress can be positive or negative for different materials, hence H_0 can be positive or negative. For $H \gg |H_0|$, the bulk material dominates the overall properties of the structure; the contribution from the surface is so small that it can be neglected. When H is comparable to $|H_0|$, the surface effects become noticeable, therefore they cannot be ignored.

2.3 Static Bending of Nanoscale Beams

In this section, several practical cases of nanoscale beams based on the beam theories derived above are solved. In the next subsections, a set of closed-form analytical solutions for static bending of thin and thick beams under different loading (point and uniformly distributed) and boundary conditions (simply-supported, cantilever and both ends clamped) as shown in Figure 2.4 are presented.

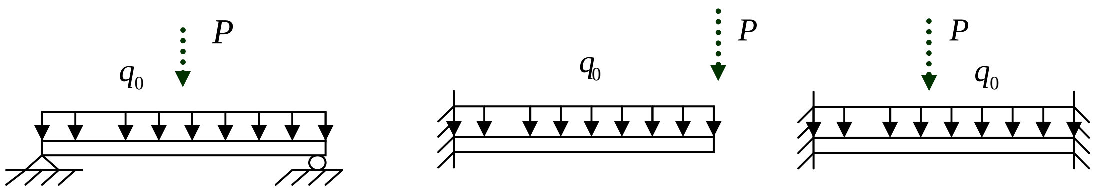

(a) simply-supported (b) cantilever (c) clamped ends

Figure 2.4 Beams under different boundary and loading conditions

2.3.1 Analytical Solutions for Thin Beam Static Bending

For the static problems, the governing equation (2.23) is further simplified to,

$$[EI+(2\mu_0+\lambda_0)I^* - \frac{2\nu I\tau_0}{H}]\frac{d^4w}{dx^4} - \tau_0 s^* \frac{d^2w}{dx^2} + q(x) = 0 \tag{2.27}$$

The non-dimensional quantities are introduced as follows,

$$\bar{x} = x/L\,, \bar{w} = w/L \text{ and } \varepsilon = \frac{\tau_0 s^*}{K_b}L^2 \tag{2.28}$$

Equation (2.27) can therefore be rewritten in terms of non-dimensional quantities $\bar{x}$ and $\bar{w}$ in the following form,

$$\frac{d^4\bar{w}}{d\bar{x}^4} - \varepsilon\frac{d^2\bar{w}}{d\bar{x}^2} + \frac{qL^3}{K_b} = 0 \tag{2.29}$$

The shear force and bending moment can also be rewritten as,

$$\begin{aligned} M^E &= \frac{-K_b}{L}\frac{d^2\bar{w}}{d\bar{x}^2} \\ Q^E &= \frac{-K_b}{L^2}\frac{d^3\bar{w}}{d\bar{x}^3} + \tau_0 s^* \frac{d\bar{w}}{d\bar{x}} \end{aligned} \tag{2.30}$$

Note that negative surface elastic constants at small dimensions could yield negative K_b, which lead to deflection instability. The reason for this phenomenon is that the non-positive definiteness of surface elastic energy will dominate over the bulk strain energy at small dimensions. In this case, the Gurtin-Murdoch theory essentially breaks down and other atomistic models need to be chosen. Our model is applicable only when the bulk is still the dominant part although the surface contribution is prominent. Therefore, the following derivations are based on the restriction $K_b > 0$.

Solving the fourth order differential equation (2.29), the general solution for a uniformly distributed load q_0 can be derived as,

$$\overline{w} = c_1 e^{\overline{x}\sqrt{\varepsilon}} + c_2 e^{-\overline{x}\sqrt{\varepsilon}} + c_3 + c_4 \overline{x} + \frac{q_0 L^3}{2K_b \varepsilon} \overline{x}^2 \tag{2.31}$$

As shown in equation (2.31), the normalized deflection contains four unknown constants, $c_1 - c_4$. These constants can be evaluated from the beam boundary conditions. In our work, three common boundary conditions for a beam subjected to uniformly distributed load and point load (Figure 2.4) are studied and the normalized deflections are presented for each case.

Simply Supported (SS) Beams

The boundary conditions for simply supported beams (Figure 2.4a) under a uniformly distributed load are given as,

$$\begin{aligned} &\overline{w}(0) = \overline{w}(1) = 0 \\ &M^E(0) = M^E(1) = 0 \end{aligned} \tag{2.32}$$

Using equations (2.30), (2.31) and the above boundary conditions, the solution for the normalized deflection of the beam under uniformly distributed load is obtained as,

$$\overline{w} = -\frac{q_0 L^3}{K_b \varepsilon^2} \left(\frac{e^{\overline{x}\sqrt{\varepsilon}}}{1 + e^{\sqrt{\varepsilon}}} + \frac{e^{-\overline{x}\sqrt{\varepsilon}}}{1 + e^{-\sqrt{\varepsilon}}} - \frac{\varepsilon}{2} \overline{x}^2 + \frac{\varepsilon}{2} \overline{x} - 1 \right) \tag{2.33}$$

Now consider the beam under a mid-point load of magnitude P. As the structure and boundary conditions are symmetric with respect to the loading plane, half beam is considered here. The boundary conditions can be expressed as,

$$\begin{aligned} &\overline{w}(0) = \overline{w}'(1/2) = 0 \\ &M^E(0) = 0 \\ &Q^E(1/2) = -P/2 \end{aligned} \tag{2.34}$$

Using equations (2.30) and (2.31) with $q_0 = 0$ and boundary conditions (2.34) yields the following solution for the four arbitrary constants.

$$c_1 = \frac{PL^2}{2K_b \varepsilon^{3/2} (e^{\sqrt{\varepsilon}/2} + e^{-\sqrt{\varepsilon}/2})} ; \; c_2 = -\frac{PL^2}{2K_b \varepsilon^{3/2} (e^{\sqrt{\varepsilon}/2} + e^{-\sqrt{\varepsilon}/2})}$$

$$c_3 = 0 ; \; c_4 = -\frac{PL^2}{2K_b \varepsilon} \tag{2.35}$$

Cantilever (C) Beams

In the case of cantilever beam (Figure 2.4b) subjected to a uniformly distributed load, the boundary conditions are,

$$\begin{aligned}&\bar{w}(0)=\bar{w}'(0)\\&M^E(1)=Q^E(1)=0\end{aligned} \tag{2.36}$$

Using the above boundary conditions and equations (2.30) and (2.31) yields the following,

$$c_1=-\frac{q_0L^3(1-e^{-\sqrt{\varepsilon}}\sqrt{\varepsilon})}{K_b\varepsilon^2(e^{\sqrt{\varepsilon}}+e^{-\sqrt{\varepsilon}})};\ c_2=-\frac{q_0L^3(1+e^{\sqrt{\varepsilon}}\sqrt{\varepsilon})}{K_b\varepsilon^2(e^{\sqrt{\varepsilon}}+e^{-\sqrt{\varepsilon}})}$$

$$c_3=\frac{q_0L^3(2+e^{\sqrt{\varepsilon}}\sqrt{\varepsilon}-e^{-\sqrt{\varepsilon}}\sqrt{\varepsilon})}{K_b\varepsilon^2(e^{\sqrt{\varepsilon}}+e^{-\sqrt{\varepsilon}})};\ c_4=-\frac{q_0L^3}{K_b\varepsilon} \tag{2.37}$$

In the case of a cantilever beam under a tip load P, the boundary conditions are given by,

$$\begin{aligned}&\bar{w}(0)=\bar{w}'(0)=0\\&M^E(1)=0\\&Q^E(1)=-P\end{aligned} \tag{2.38}$$

The solutions for the four unknowns can be derived as,

$$c_1=\frac{PL^2}{K_b\varepsilon^{3/2}(e^{2\sqrt{\varepsilon}}+1)};\ c_2=-\frac{PL^2e^{2\sqrt{\varepsilon}}}{K_b\varepsilon^{3/2}(e^{2\sqrt{\varepsilon}}+1)}$$

$$c_3=\frac{PL^2(e^{2\sqrt{\varepsilon}}-1)}{K_b\varepsilon^{3/2}(e^{2\sqrt{\varepsilon}}+1)};\quad c_4=-\frac{PL^2}{K_b\varepsilon} \tag{2.39}$$

Clamped-Clamped (CC) Beam

For the clamped-clamped beam (Figure 2.4c) under a uniformly distributed load, the boundary conditions are,

$$\begin{aligned}&\bar{w}(0)=\bar{w}'(0)=0\\&\bar{w}(1)=\bar{w}'(1)=0\end{aligned} \tag{2.40}$$

Solving equation (2.31) with the boundary conditions, the four unknown constants are obtained as,

$$c_1=-\frac{q_0L^3}{2K_b\varepsilon^{3/2}(e^{\sqrt{\varepsilon}}-1)};\ c_2=-\frac{q_0L^3e^{\sqrt{\varepsilon}}}{2K_b\varepsilon^{3/2}(e^{\sqrt{\varepsilon}}-1)}$$

$$c_3 = \frac{q_0 L^3 (e^{\sqrt{\varepsilon}} + 1)}{2K_b \varepsilon^{3/2} (e^{\sqrt{\varepsilon}} - 1)}\,;\ c_4 = -\frac{q_0 L^3}{K_b \varepsilon} \tag{2.41}$$

In the case of clamped-clamped beam under a mid-point load P, as the loading and boundary conditions are symmetric, half of the beam is considered. Therefore the boundary conditions are given by,

$$\begin{aligned} &\overline{w}(0) = \overline{w}'(0) = \overline{w}'(1/2) = 0 \\ &Q^E(1/2) = -P/2 \end{aligned} \tag{2.42}$$

The solutions for the arbitrary constants are,

$$c_1 = \frac{PL^2 e^{-\sqrt{\varepsilon}/2}}{2K_b \varepsilon^{3/2} (e^{-\sqrt{\varepsilon}/2} + 1)}\,;\ c_2 = -\frac{PL^2}{2K_b \varepsilon^{3/2} (e^{-\sqrt{\varepsilon}/2} + 1)}$$

$$c_3 = \frac{PL^2 (1 - e^{-\sqrt{\varepsilon}/2})}{2K_b \varepsilon^{3/2} (e^{-\sqrt{\varepsilon}/2} + 1)}\,;\ \ c_4 = -\frac{PL^2}{2K_b \varepsilon} \tag{2.43}$$

The above closed-form analytical results clearly show that the deflections of the thin beams are influenced by the surface energy in terms of the modified bending stiffness K_b and the non-dimensional material constant ε. A further quantitative study of such surface effects is presented in the ensuing section dealing with numerical results.

2.3.2 Analytical Solutions for Thick Beam Static Bending

In some practical situations where the beam aspect ratio is relatively small (e.g. $L/H < 10$), the thick beam model needs to be applied to take the shear deformations into consideration. The governing equations for thick beam static bending can be simplified from equations (2.18) and (2.19) as,

$$G\kappa A\left(\frac{d^2 w}{dx^2} + \frac{d\phi}{dx}\right) + \tau_0 s^* \frac{d^2 w}{dx^2} - q(x) = 0 \tag{2.44}$$

$$[EI + (2\mu_0 + \lambda_0) I^*] \frac{d^2 \phi}{dx^2} + \frac{2\nu I \tau_0}{H} \frac{d^3 w}{dx^3} - G\kappa A\left(\frac{dw}{dx} + \phi\right) = 0 \tag{2.45}$$

Following the procedure in thin beam, rewrite above governing equations in terms of the non-dimensional quantities $\overline{w}$ and $\overline{x}$ as,

$$G\kappa A\left(\frac{d^2 \overline{w}}{d\overline{x}^2} + \frac{d\phi}{d\overline{x}}\right) + \tau_0 s^* \frac{d^2 \overline{w}}{d\overline{x}^2} - q(\overline{x}) L = 0 \tag{2.46}$$

$$[EI+(2\mu_0+\lambda_0)I^*]\frac{d^2\phi}{d\overline{x}^2}+\frac{2\nu I\tau_0}{H}\frac{d^3\overline{w}}{d\overline{x}^3}-G\kappa AL^2(\frac{d\overline{w}}{d\overline{x}}+\phi)=0 \tag{2.47}$$

The angular displacement ϕ can be expressed in terms of $\overline{w}$ by using equation (2.46) for a uniformly distributed load q_0 as,

$$\phi=-\frac{1}{G\kappa A}[(G\kappa A+\tau_0 s^*)\frac{d\overline{w}}{d\overline{x}}-q_0L\overline{x}+C_4] \tag{2.48}$$

where C_4 is an arbitrary constant obtained from the integral.

Substitution of equation (2.48) into (2.47) yields,

$$\frac{d^3\overline{w}}{d\overline{x}^3}-\xi\frac{d\overline{w}}{d\overline{x}}+\frac{q_0L^3}{K_s}\overline{x}-\frac{C_4L^2}{K_s}=0 \tag{2.49}$$

where $K_s=[EI+(2\mu_0+\lambda_0)I^*](1+\frac{\tau_0 s^*}{G\kappa A})-\frac{2\nu I\tau_0}{H}$ and $\xi=\frac{\tau_0 s^*}{K_s}L^2$. Analogy to thin beam case, $K_s>0$ is assumed in the following derivations.

The general solution of equation (2.49) is,

$$\overline{w}=C_1e^{\overline{x}\sqrt{\xi}}+C_2e^{-\overline{x}\sqrt{\xi}}+C_3+\frac{q_0L^3}{2K_s\xi}\overline{x}^2-\frac{C_4L^2}{K_s\xi}\overline{x} \tag{2.50}$$

Using equations (2.48) and (2.50), the solution for the angular displacement can be derived as,

$$\phi=-(1+\frac{\tau_0 s^*}{G\kappa A})\sqrt{\xi}(C_1e^{\overline{x}\sqrt{\xi}}-C_2e^{-\overline{x}\sqrt{\xi}})-\frac{q_0L^3}{K_s\xi}\overline{x}+\frac{C_4L^2}{K_s\xi} \tag{2.51}$$

where C_1 to C_4 are unknowns to be determined by the boundary conditions. Meanwhile, the resultant shear force and bending moment can be simplified from equation (2.21) as,

$$\begin{aligned} Q^T &= G\kappa A(\frac{\partial w}{\partial x}+\phi)+\tau_0 s^*\frac{\partial w}{\partial x} \\ M^T &= [EI+I^*(2\mu_0+\lambda_0)I^*]\frac{\partial\phi}{\partial x}+\frac{2\nu I\tau_0}{H}\frac{\partial^2 w}{\partial x^2} \end{aligned} \tag{2.52}$$

Analogous to thin beam case, in the rest of this section, three beam supported cases (Figure 2.4) under uniformly distributed load and point load are studied and the normalized deflections of thick beams with surface effects are presented.

Simply Supported (SS) Beams

For a simply supported beam, the boundary conditions are given in equation (2.32). Substituting the general solutions (2.50) and (2.51) into the boundary conditions together with equation (2.52), the four arbitrary unknowns are obtained as the following,

$$C_1 = -\frac{K_b q_0 L^3 (1 - e^{-\sqrt{\xi}})}{K_s^2 \xi^2 (e^{\sqrt{\xi}} - e^{-\sqrt{\xi}})};\ C_2 = -\frac{K_b q_0 L^3 (e^{\sqrt{\xi}} - 1)}{K_s^2 \xi^2 (e^{\sqrt{\xi}} - e^{-\sqrt{\xi}})}$$

$$C_3 = \frac{K_b q_0 L^3}{K_s^2 \xi^2};\ C_4 = \frac{q_0 L}{2} \tag{2.53}$$

For a simply supported beam subjected to a mid-point load of magnitude P, the boundary conditions for half beam are shown in equation (2.34). Setting q_0 to zero in equations (2.50) and (2.51) and then substituting them into the boundary conditions leads to,

$$C_1 = \frac{PL^2}{2K_s \xi^{3/2} (1 + \frac{\tau_0 s^*}{G\kappa A})(e^{\sqrt{\xi}/2} + e^{-\sqrt{\xi}/2})}$$

$$C_2 = -\frac{PL^2}{2K_s \xi^{3/2} (1 + \frac{\tau_0 s^*}{G\kappa A})(e^{\sqrt{\xi}/2} + e^{-\sqrt{\xi}/2})}$$

$$C_3 = 0$$

$$C_4 = \frac{P}{2} \tag{2.54}$$

Cantilever (C) Beams

In the case of cantilever beam under uniformly distributed load, the solutions can be obtained by using boundary conditions given in equation (2.36) as,

$$C_1 = \frac{q_0 L^3}{K_s \xi} \left(\frac{e^{-\sqrt{\xi}}}{\sqrt{\xi}(1 + \frac{\tau_0 s^*}{G\kappa A})} - \frac{K_b}{K_s \xi} \right) / (e^{\sqrt{\xi}} + e^{-\sqrt{\xi}})$$

$$C_2 = -\frac{q_0 L^3}{K_s \xi} \left(\frac{e^{\sqrt{\xi}}}{\sqrt{\xi}(1 + \frac{\tau_0 s^*}{G\kappa A})} + \frac{K_b}{K_s \xi} \right) / (e^{\sqrt{\xi}} + e^{-\sqrt{\xi}})$$

$$C_3 = \frac{q_0 L^3}{K_s \xi}\left(\frac{(e^{\sqrt{\xi}} - e^{-\sqrt{\xi}})}{\sqrt{\xi}(1+\frac{\tau_0 s^*}{G\kappa A})} + \frac{2K_b}{K_s \xi}\right) / (e^{\sqrt{\xi}} + e^{-\sqrt{\xi}})$$

$$C_4 = q_0 L \tag{2.55}$$

In the case of a cantilever beam subjected to a point load P at the free end, the solution is derived as,

$$C_1 = \frac{PL^2 e^{-\sqrt{\xi}}}{K_s \xi^{3/2}(1+\frac{\tau_0 s^*}{G\kappa A})(e^{\sqrt{\xi}} + e^{-\sqrt{\xi}})}$$

$$C_2 = -\frac{PL^2 e^{\sqrt{\xi}}}{K_s \xi^{3/2}(1+\frac{\tau_0 s^*}{G\kappa A})(e^{\sqrt{\xi}} + e^{-\sqrt{\xi}})}$$

$$C_3 = \frac{PL^2 (e^{\sqrt{\xi}} - e^{-\sqrt{\xi}})}{K_s \xi^{3/2}(1+\frac{\tau_0 s^*}{G\kappa A})(e^{\sqrt{\xi}} + e^{-\sqrt{\xi}})}$$

$$C_4 = P \tag{2.56}$$

Clamped-Clamped (CC) Beam

For a clamped-clamped beam with a uniformly distributed load, using the boundary conditions in equation (2.40), the solution for arbitrary constants is given by,

$$C_1 = -\frac{q_0 L^3}{2K_s \xi^{3/2}(1+\frac{\tau_0 s^*}{G\kappa A})(e^{\sqrt{\xi}} - 1)}$$

$$C_2 = -\frac{q_0 L^3 e^{\sqrt{\xi}}}{2K_s \xi^{3/2}(1+\frac{\tau_0 s^*}{G\kappa A})(e^{\sqrt{\xi}} - 1)}$$

$$C_3 = \frac{q_0 L^3 (e^{\sqrt{\xi}} + 1)}{2K_s \xi^{3/2}(1+\frac{\tau_0 s^*}{G\kappa A})(e^{\sqrt{\xi}} - 1)}$$

$$C_4 = \frac{q_0 L}{2} \tag{2.57}$$

For a clamped-clamped beam subjected to a midpoint load of magnitude P, the solution is derived by using boundary conditions (2.42),

$$C_1 = \frac{PL^2(1-e^{-\sqrt{\xi}/2})}{2K_s\xi^{3/2}(1+\frac{\tau_0 s^*}{G\kappa A})(e^{\sqrt{\xi}/2}-e^{-\sqrt{\xi}/2})}$$

$$C_2 = \frac{PL^2(1-e^{\sqrt{\xi}/2})}{2K_s\xi^{3/2}(1+\frac{\tau_0 s^*}{G\kappa A})(e^{\sqrt{\xi}/2}-e^{-\sqrt{\xi}/2})}$$

$$C_3 = \frac{PL^2(e^{\sqrt{\xi}/2}+e^{-\sqrt{\xi}/2}-2)}{2K_s\xi^{3/2}(1+\frac{\tau_0 s^*}{G\kappa A})(e^{\sqrt{\xi}/2}-e^{-\sqrt{\xi}/2})}$$

$$C_4 = \frac{P}{2} \tag{2.58}$$

Again it is noted that the deflections of the thick beam are dependent on the two parameters ξ and K_s which are the representations of the surface energy effects.

2.4 Buckling of Nanoscale Beams

In the preceding sections, we have discussed the methods to determine the beam deflections, tacitly assuming that the beams were always in stable equilibrium. Some nanoscale beams exploited in NEMS devices, however, are often subjected to compressive axial forces. If these compressive forces exceed a critical force, they will cause the beams to buckle. Quite often the buckling can lead to a dramatic failure of the mechanism of the devices. As a result, the critical loads need to be examined to assure the structural stability. This section begins with a general discussion of the nanoscale beam deformation under compression with surface effects incorporated, followed by the determination of the critical loads for different beam restraints.

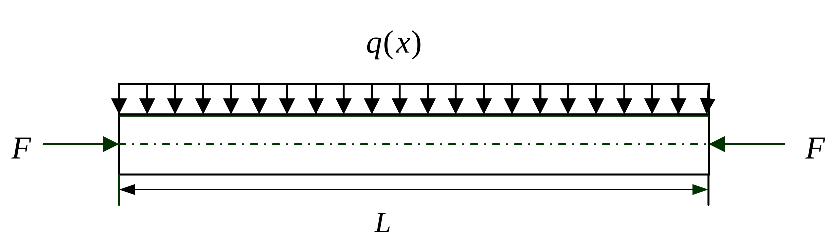

Figure 2.5 Geometry and loading conditions of beam for axial buckling

2.4.1 Modified Thin Beam Model for Axial Buckling

In conventional continuum mechanics, the buckling of a beam under compressive force was first derived by Euler [51]. To incorporate the surface effects into the conventional theory, based on the thin beam model (modified Euler-Bernoulli beam theory) obtained in last section, an axial force F (positive in compression) is added to the beam configuration as shown in Figure 2.5. Consequently, the differential equation (2.27) needs to be modified by the presence of the compressive force as,

$$[EI+(2\mu_0+\lambda_0)I^*-\frac{2\nu I\tau_0}{H}]\frac{\partial^4 w}{\partial x^4}+(F-\tau_0 s^*)\frac{\partial^2 w}{\partial x^2}+q(x)=0 \tag{2.59}$$

Equation (2.59) is the general differential equation for the deflections of a beam-column considering surface effects. It is an ordinary linear differential equation of fourth order. Its general solution can be derived as,

$$w(x)=C_1\cos\beta x+C_2\sin\beta x+C_3 x+C_4+w_q(x) \tag{2.60}$$

where $\beta=\sqrt{\dfrac{F-\tau_0 s^*}{EI+(2\mu_0+\lambda_0)I^*-\dfrac{2\nu I\tau_0}{H}}}$, C_1-C_4 are arbitrary constants that must be determined by appropriate boundary conditions. $w_q(x)$ is a particular solution corresponding to the transverse loading $q(x)$, which can be ignored in the process of determining the critical loads. The critical loads of beams with different restraints are elaborated in the following subsection.

2.4.2 Critical Loads for Beam with Different Restraints

Simply supported (SS) beam

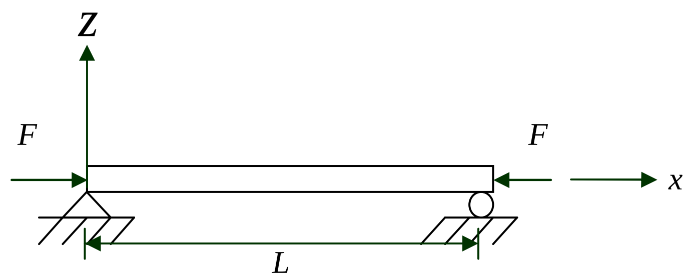

Figure 2.6 Configuration of simply supported beam under compression

Figure 2.6 shows a compressed simply supported beam. The boundary conditions are given as $w(0)=w(L)=0, M^E(0)=M^E(L)=0$. Substituting the boundary conditions to equation (2.60) gives,

$$C_1 + C_4 = 0$$

$$-\beta^2 C_1 = 0$$

$$C_1 \cos\beta L + C_2 \sin\beta L + C_3 L + C_4 = 0 \tag{2.61}$$

$$-C_1\beta^2 \cos\beta L - C_2\beta^2 \sin\beta L = 0$$

Solving above equations yields $\sin\beta L = 0$ for a nontrivial solution, so

$$\beta L = n\pi, \; n = 1, 2, 3, \ldots \tag{2.62}$$

The critical load is derived when $n = 1$,

$$F_{cr} = \frac{\pi^2 (EI + (2\mu_0 + \lambda_0) I^* - \frac{2\nu I \tau_0}{H})}{L^2} + \tau_0 s^* \tag{2.63}$$

Cantilever beam

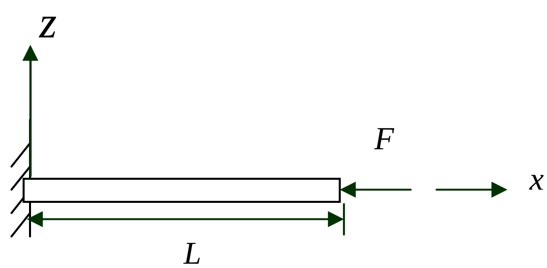

Figure 2.7 Configuration of cantilever beam under compression

For the cantilever beam, the boundary conditions are given as $w(0) = w'(0), M^E(L) = Q^E(L) = 0$. Substitution of the boundary conditions into the general equation leads to,

$$C_1 + C_4 = 0$$

$$\beta C_2 + C_3 = 0$$

$$-C_1\beta^2 \cos\beta L - C_2\beta^2 \sin\beta L = 0 \tag{2.64}$$

$$(EI + (2\mu_0 + \lambda_0) I^* - \frac{2\nu I \tau_0}{H})(C_1\beta^3 \sin\beta L - C_2\beta^3 \cos\beta L)$$

$$+(F - \tau_0 s^*)(-C_1\beta \sin\beta L + C_2\beta \cos\beta L + C_3) = 0$$

Solving the above equations yields $\cos\beta L = 0$ for nontrivial solution, so

$$\beta L = \frac{(2n-1)\pi}{2}, \; n = 1, 2, 3.... \tag{2.65}$$

Thus, the critical force is obtained as,

$$F_{cr} = \frac{\pi^2 (EI + (2\mu_0 + \lambda_0) I^* - \frac{2\nu I \tau_0}{H})}{4L^2} + \tau_0 s^* \tag{2.66}$$

Clamped-clamped ends beam

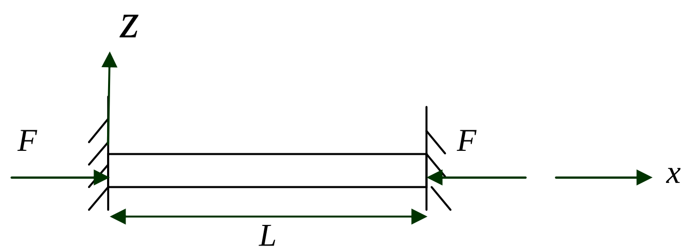

Figure 2.8 Configuration of clamped-clamped ends beam under compression

For the both end clamped beam, the boundary conditions are given as, $w(0) = w'(0) = 0, w(L) = w'(L) = 0$. Substitution of the boundary conditions into the general solution yields the following expressions,

$$C_1 + C_4 = 0$$

$$C_2 \beta + C_3 = 0$$

$$C_1 \cos\beta L + C_2 \sin\beta L + C_3 L + C_4 = 0 \tag{2.67}$$

$$-C_1 \beta \sin\beta L + C_2 \beta \cos\beta L + C_3 = 0$$

The existence of non trivial solution requires,

$$\sin\frac{\beta L}{2} \left(\frac{\beta L}{2} \cos\frac{\beta L}{2} - \sin\frac{\beta L}{2}\right) = 0 \tag{2.68}$$

Equation (2.68) is satisfied by,

$$\sin\frac{\beta L}{2} = 0 \tag{2.69}$$

or $$\frac{\beta L}{2} = \tan\frac{\beta L}{2} \tag{2.70}$$

The critical force obtained from equation (2.69) is,

$$F_{cr} = \frac{4\pi^2(EI + (2\mu_0 + \lambda_0)I^* - \frac{2\nu I\tau_0}{H})}{L^2} + \tau_0 s^* \tag{2.71}$$

Solving (2.70) numerically leads to another critical force as,

$$F_{cr} = \frac{8.18\pi^2(EI + (2\mu_0 + \lambda_0)I^* - \frac{2\nu I\tau_0}{H})}{L^2} + \tau_0 s^* \tag{2.72}$$

Since the value of (2.71) is bigger than (2.72), so for general buckling cases, the critical force is taken the smaller value as shown in (2.71).

Based on the above derivation, the critical load of axial buckling of nanoscale beam can be written as,

$$F_{cr} = \frac{a\pi^2 K_b}{L^2} + \mathrm{T} \tag{2.73}$$

a is a coefficient that must be determined according to the boundary conditions. The derivation indicates that a still takes the value given in classical theory of Euler beams. K_b is the modified bending stiffness. T is a constant determined by the surface residual stress and the geometry of cross section.

2.5 Numerical Results for Nanoscale Beam Static Response

In this section, selected numerical results are presented to demonstrate the salient features of mechanical behavior of nanoscale beams with rectangular cross-section and the effects of surface energy for different beam boundary conditions. Beams made of aluminum (Al) and silicon (Si) are considered in the numerical study. The bulk properties and surface properties for [1 0 0] surface of selected materials have been obtained by Miller and Shenoy [16, 17] by using the embedded atom method proposed by Daw and Baskes [54]. The results are as shown in Table 2.1. The dimensions for thin beams are $L = 120nm$, $H = 2h = 6nm$ and $b = 3nm$, and those for thick beams are $L = 50nm$, $H = 2h = 6nm$ and $b = 3nm$ in all the calculations of static bending.

Table 2.1 Material Properties of Aluminum and Silicon

Material	E (Gpa)	v	μ_0 (N/m)	λ_0 (N/m)	τ_0 (N/m)	ρ (kg/m^3)	ρ_0 (kg/m^2)
Al	90	0.23	-5.4251	3.4939	0.5689	2.7×10^3	5.46×10^{-7}
Si	107	0.33	-2.7779	-4.4939	0.6056	2.33×10^3	3.17×10^{-7}

Based on the analysis presented in section 2.3, it is seen from equations (2.29) and (2.49), the influence of surface energy is reflected in the constants K_b and ε in the case of thin beam; K_s and ξ in the case of thick beam respectively. If the surface energy effects are completely neglected, K_b and K_s will reduce to the classical bending stiffness EI , ε and ξ will vanish. To get a quantitative assessment of the effects of surface energy, the deflection profiles of thin Al and Si beams for the three common boundary conditions (SS, C and CC) are plotted in Figure 2.9. For generality, the normalized deflections, $W_q^E = w/(q_0L)$ and $W_p^E = w/P$ are used. Solutions are presented for a uniformly distributed load (q_0) as well as a mid-point concentrated load (P) for SS and CC beams and an end point load for a C beam. The deflections with surface effects are also compared with those of identical beams based on classical beam theory (no surface effects). From Figure 2.9, it can be seen that surface energy effects have a substantial influence on the deflections on Al and Si beams. This behavior can also be interpreted by the intrinsic length scale defined in equation (2.26). The intrinsic lengths $|\alpha H_0|$ for Al and Si beams of aforementioned dimensions are 8.20$\overset{\circ}{\mathrm{A}}$ and 9.43$\overset{\circ}{\mathrm{A}}$ respectively. The beam heights are comparable to the intrinsic lengths, therefore the surface energy effects are pronounced in both cases. It is also found that when the surface parameters are neglected in the thin beam model, the deflection curves of thin beam model will overlap with those from classical beam theory.

Reconsider the surface effect factors K_b and ε for thin beam model as shown in equations (2.25) and (2.28) respectively. It may be noted that positive μ_0 and λ_0 increase K_b and consequently decrease the deflections when compared to bending stiffness EI and the corresponding deflections in the classical beam theory respectively (and vice versa for negative μ_0 and λ_0). This is confirmed in Figure 2.10(a) where the normalized deflections of a half Si SS beam under different values of $2\mu_0 + \lambda_0$ are compared with the classical result ($2\mu_0 + \lambda_0 = 0$). It is also found that the contribution of τ_0 to K_b is trivial, which implies that the influence of vertical stress σ_{zz} on the beam deformation is very small and can be neglected for all practical purposes. However, τ_0 has a more significant influence on the dimensionless factor ε. The value of ε can be positive or negative depending on the positive and negative τ_0 and its value is controlled by τ_0 as well. Figure 2.10 (b) shows the influence of ε on the beam deformations by changing τ_0 in a reasonable range and setting μ_0 and λ_0 to zero. It can be seen that positive ε increases the overall bending stiffness and negative ε decreases the overall bending stiffness.

For slender beams with aspect ratio $L/H > 20$, thin beam model is sufficient to predict the beam behavior with a good accuracy [52]. As the aspect ratio decreases, the shear deformation and rotary inertia become important, the thick beam model needs to be used. However, it is found that for beams with aspect ratio $10 \le L/H \le 20$ the difference between maximum deflections corresponding to thin and thick beam theories is less than 5% and thick beam theory is therefore needed when $L/H < 10$.

Figure 2.11 shows the solutions for Al and Si thick beams. The same loading and boundary conditions and normalized deflections are used as those in thin beams. The incorporation of shear deformations increases the beam flexibility and the deflections predicted by thick beam theory are therefore larger than the corresponding results from thin beam theory. In the case of thick beams, the difference between the deflections of the present model and classical thick beam model becomes comparatively less compared to the case of thin beams. The underlying reason can be explained to the energy point of view. With the consideration of shear deformation in thick beam model, a larger portion of the total energy will distribute in the bulk compared to that in thin beam model, therefore the energy stored on the surface will become less, which results in weaker surface effects on the thick beams.

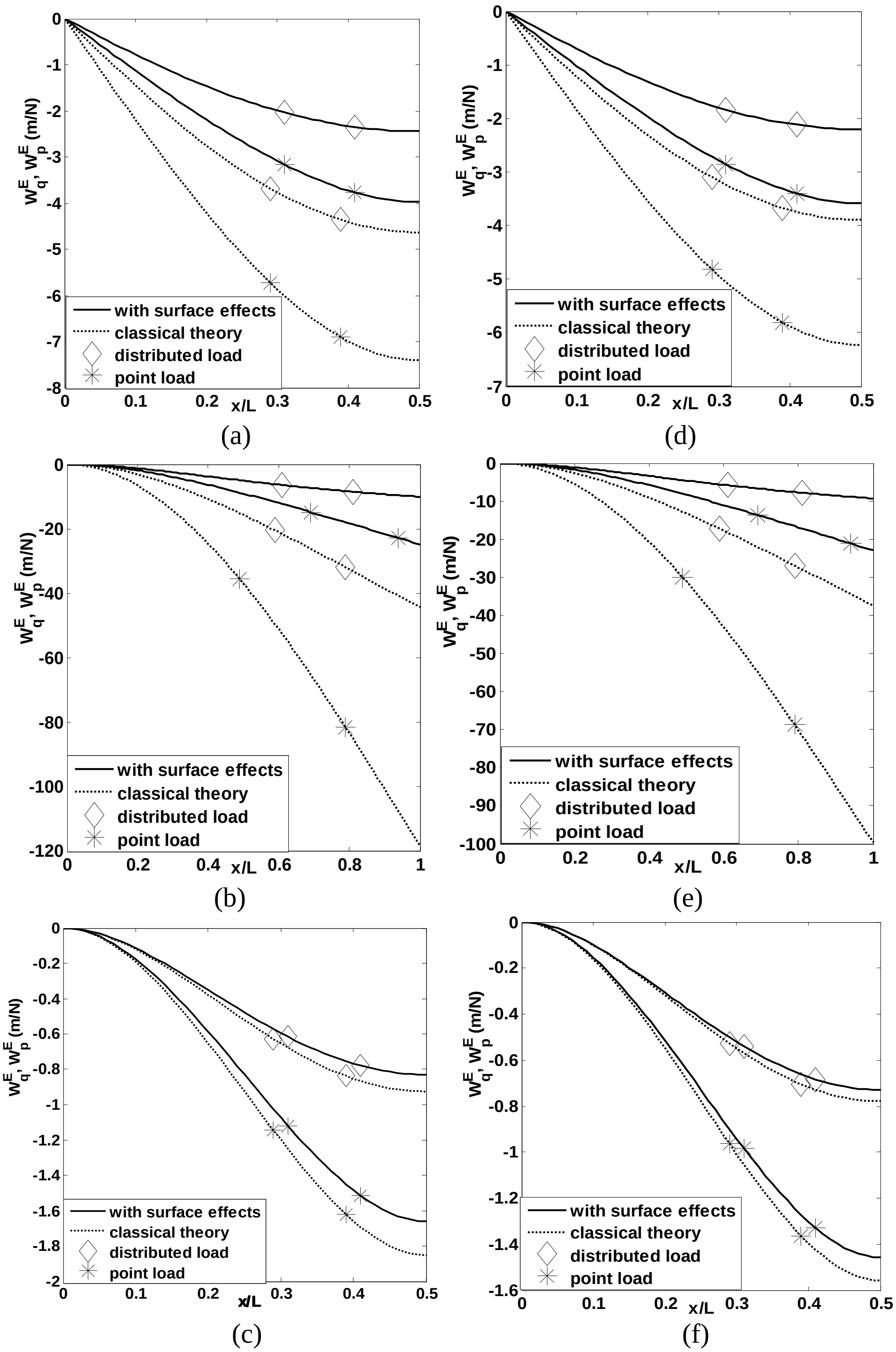

Figure 2.9 Normalized deflections of thin beams under point and distributed loads; (a) Al simply supported (b) Al cantilever (c) Al clamped-clamped ends (d) Si simply supported (e) Si cantilever (f) Si clamped-clamped ends.

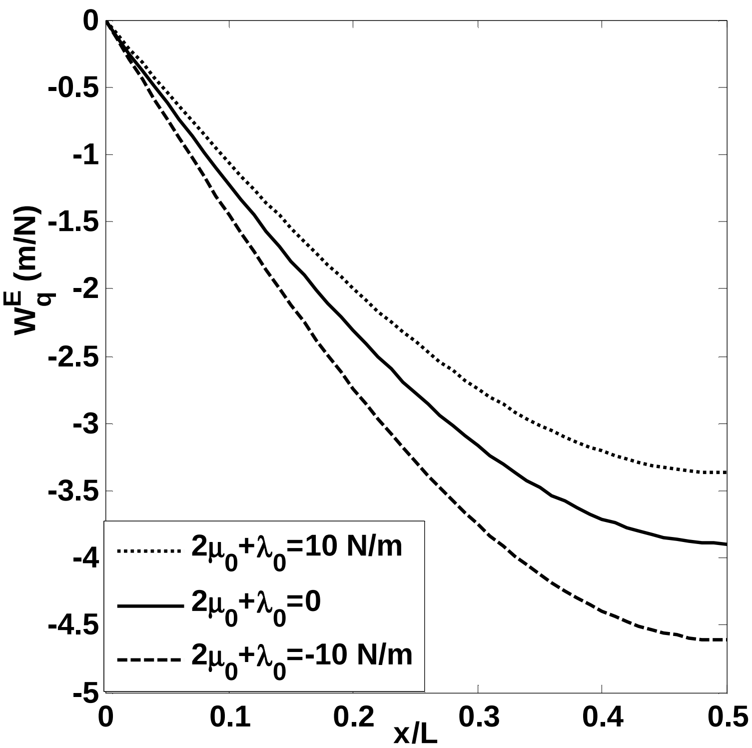

(a)

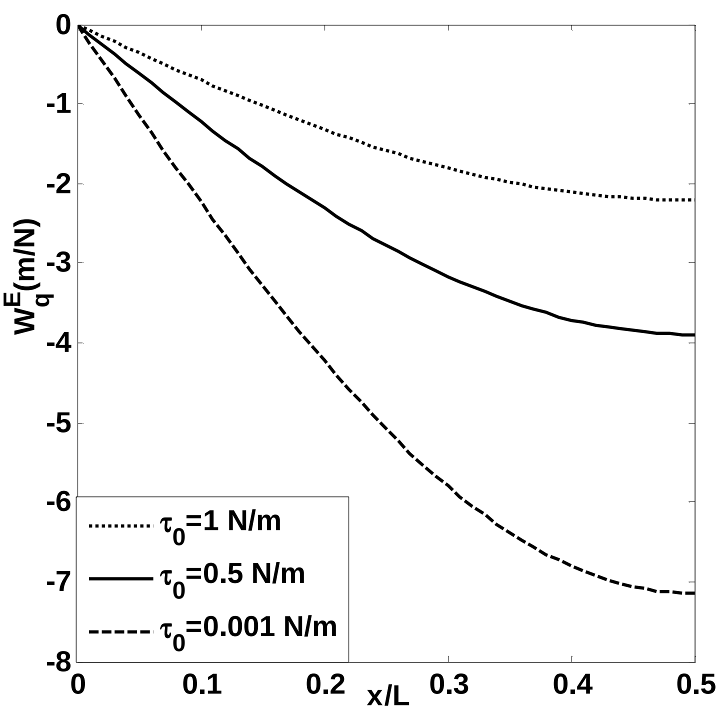

(b)

Figure 2.10 Normalized deflections of half Si simply supported beam under uniformly distributed load. (a) $2\mu_0 + \lambda_0$ varies, $\varepsilon \to 0$ (b) τ_0 varies, $\mu_0 = \lambda_0 = 0$.

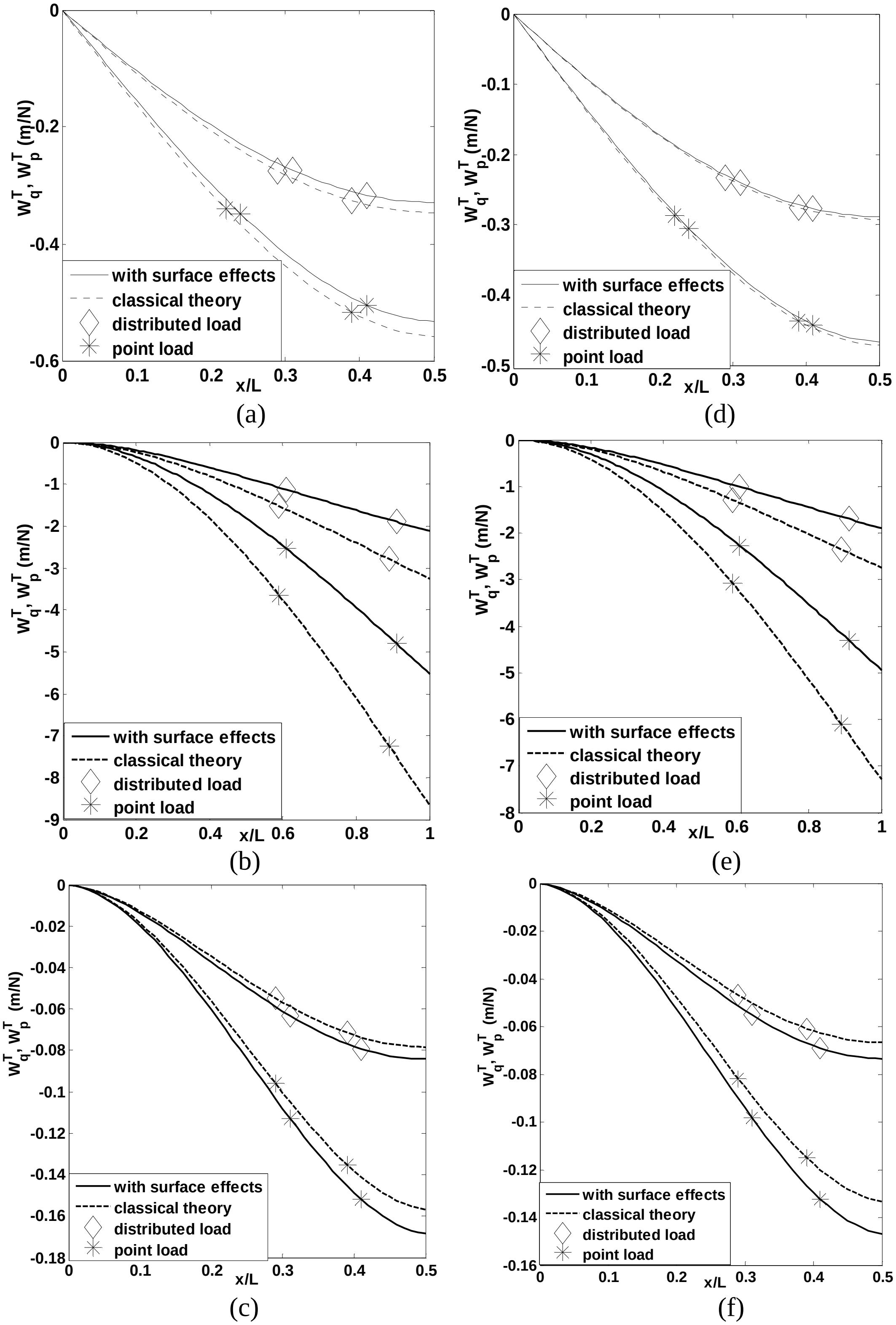

Fig. 2.11 Normalized deflections of thick beams under point and distributed loads; (a) Al simply supported (b) Al cantilever (c) Al clamped-clamped ends (d) Si simply supported (e) Si cantilever (f) Si clamped-clamped ends

A review of Figures 2.9 and 2.11 shows that the end boundary conditions affect the influence of surface energy. For example, a CC thin Si beam shows a relatively small influence of surface energy effects whereas both SS and C Al beams show a substantial influence. The influence of surface energy becomes more important as the surface strains become larger due to increasing deflections.

The critical loads of Al and Si beams under above mentioned restraints are calculated and compared with those from classical theory. In the calculation, beams with $L = 200nm$, $H = 2h = 10nm$ and $b = 10nm$ are used. Table 2.2 shows the results using the surface elastic model, followed by those using classical theory in square brackets. It can be seen that the magnitude of critical loads could be significantly influenced by the presence of surface effects. They could either be increased or decreased compared to the classical results depending on the signs of surface elastic constants and surface residual stress. In the cases of Al and Si, the critical loads are shown to be increased due to the positive surface residual stress. Accuracy of the numerical calculations is confirmed by setting the surface properties in surface elastic solutions to zero and comparing them with the classical solutions. It is found that the results are identical. It can also be seen that the significance of surface energy effects also depends on the boundary conditions. The largest influence is observed for cantilever beam. This is consistent with the results observed in static bending. Figure 2.12 shows the non-dimensional difference of critical load of Si simply supported beam with above mentioned dimensions from surface elastic model and classical theory. It can be seen that the influence of surface effects on critical load becomes more prominent as the beam height decreases.

Table 2.2 Critical loads for beams under different boundary conditions

Beam type	Critical load (nN)	
	Al	Si
	28.67 [18.51]	32.45 [22.00]
	15.70 [4.63]	17.20 [5.50]
	80.53 [74.02]	93.47 [88.00]

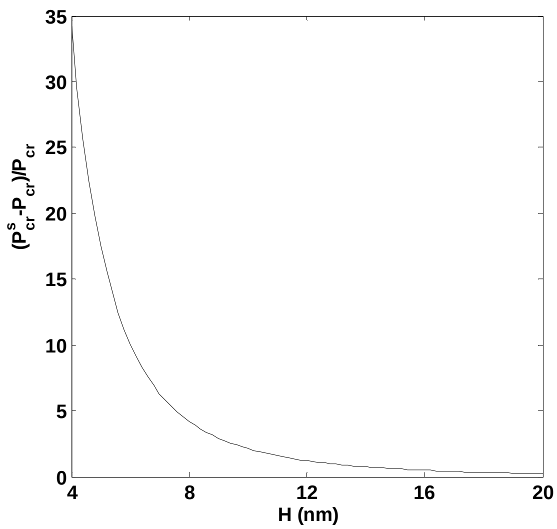

Figure 2.12 Non-dimensional differences between critical load predicted by surface elastic model and classical theory

Chapter 3

DYNAMIC ANALYSIS OF NANOSCALE BEAMS

3.1 Free Vibration of Nanoscale Beams

The free vibration characteristics (natural frequencies and mode shapes) of nanoscale beams are essential in the NEMS device design. Although the closed-form solutions for natural frequencies cannot be obtained due to the complexity of the configurations, characteristic equations for free vibration of thin and thick beams including surface effects are presented and the corresponding mode shapes are studied in this chapter.

3.1.1 Thin Beam Free Vibration

From equation (2.23), the equation of motion for thin beam free vibration can be written as,

$$K_b \frac{\partial^4 w}{\partial x^4} - \tau_0 s^* \frac{\partial^2 w}{\partial x^2} + M^* \frac{\partial^2 w}{\partial t^2} + I^0 \frac{\partial^4 w}{\partial x^2 \partial t^2} = 0 \tag{3.1}$$

where $M^* = (\rho A + \rho_0 s^*)$, $I^0 = \dfrac{2\nu I \rho_0}{H}$.

Assume the transverse deflection is in the form as,

$$w(x,t) = W(x) \sin \omega t \tag{3.2}$$

where $W(x)$ is the transverse vibration mode, ω is the natural frequency. By substituting equation (3.2) into equation (3.1), the equation of motion becomes,

$$\frac{d^4 W}{dx^4} - \eta_1 \frac{d^2 W}{dx^2} - \eta_2 W = 0 \tag{3.3}$$

where $\eta_1 = \dfrac{\tau_0 s^* + I^0 \omega^2}{K_b}$ and $\eta_2 = \dfrac{M^* \omega^2}{K_b}$.

The general solution of equation (3.3) can be written as,

$$W(x) = c_1 \sin \lambda_1 x + c_2 \cos \lambda_1 x + c_3 \sinh \lambda_2 x + c_4 \cosh \lambda_2 x \tag{3.4}$$

where c_i ($i = 1, 2, 3, 4$) are arbitrary constants. λ_1 and λ_2 are given by,

$$\lambda_1 = \left(\frac{-\eta_1 + \sqrt{\eta_1^2 + 4\eta_2}}{2}\right)^{\frac{1}{2}}, \lambda_2 = \left(\frac{\eta_1 + \sqrt{\eta_1^2 + 4\eta_2}}{2}\right)^{\frac{1}{2}} \tag{3.5}$$

The value of ω and three of the four arbitrary unknowns can be determined from the boundary conditions. For the three types of beams given in last chapter, the solutions are obtained as follows,

Simply Supported (SS) Beams

For a simply supported beam, substitution of the general solution (3.4) to the boundary conditions given in equation (2.32) together with equation (2.24) yields $c_2 = c_3 = c_4 = 0$. The natural frequencies can further be calculated as,

$$\omega_n^2 = \frac{K_b(\frac{n\pi}{L})^4 + \tau_0 s^*(\frac{n\pi}{L})^2}{M^* - I^0(\frac{n\pi}{L})^2}, \quad n = 1, 2, ... \tag{3.6}$$

For comparison, the classical natural frequencies are obtained by setting the surface parameters to zero as, $\omega_n^2 = EI(\frac{n\pi}{L})^4 \big/ M$.

Cantilever (C) Beams

For a cantilever beam, the boundary conditions (2.36) together with equation (2.24) lead to the following characteristic equation from which the natural frequencies can be determined.

$$\begin{aligned}
&\lambda_1 R_2(-K_b\lambda_2^3 + \lambda_2 R_3) + \lambda_2 R_1(K_b\lambda_1^3 + \lambda_1 R_3) \\
&\quad -[\lambda_2 R_1(-K_b\lambda_2^3 + \lambda_2 R_3) - \lambda_1 R_2(K_b\lambda_1^3 + \lambda_1 R_3)]\sin\lambda_1 L \sinh\lambda_2 L \\
&\quad -[\lambda_2 R_2(K_b\lambda_1^3 + \lambda_1 R_3) + \lambda_1 R_1(K_b\lambda_2^3 - \lambda_2 R_3)]\cos\lambda_1 L \cosh\lambda_2 L = 0
\end{aligned} \tag{3.7}$$

where $R_1 = (K_b\lambda_1^2 + I^0\omega^2)$, $R_2 = (-K_b\lambda_2^2 + I^0\omega^2)$ and $R_3 = \tau_0 s^* + I^0\omega^2$.

Clamped-Clamped (CC) Beam

For the clamped-clamped beam, repeating the same procedure, the characteristic equation can be obtained as,

$$2\lambda_1 + (\lambda_2 - \frac{\lambda_1^2}{\lambda_2})\sin\lambda_1 L \sinh\lambda_2 L - 2\lambda_1\cos\lambda_1 L \cosh\lambda_2 L = 0 \tag{3.8}$$

The characteristic equations contain the only unknown ω. Therefore, by solving the characteristic equations numerically, the natural frequencies of each case can be obtained. Subsequently, the individual mode shapes of vibration $W(x)$ can be calculated. As only three of the four arbitrary unknowns in equation (3.4) can be determined. The fourth unknown becomes the arbitrary magnitude of the eigenfunction (It is assumed to be unit in our derivations). Table 3.1 summarizes the mode shapes for three boundary configurations.

Table 3.1 Mode shapes of thin beams in various boundary configurations

Configuration	Mode shape	Coefficient A_n
Thin SS	$\sin\lambda_1 x = 0$	None
Thin C	$\cosh\lambda_2 x - \cos\lambda_1 x - A_n(\sinh\lambda_2 x - \frac{\lambda_2}{\lambda_1}\sin\lambda_1 x)$	$\dfrac{R_1\cos\lambda_1 l - R_2\cosh\lambda_2 l}{\frac{\lambda_2}{\lambda_1}R_1\sin\lambda_1 l - R_2\sinh\lambda_2 l}$
Thin CC	$\cosh\lambda_2 x - \cos\lambda_1 x - A_n(\sinh\lambda_2 x - \frac{\lambda_2}{\lambda_1}\sin\lambda_1 x)$	$\dfrac{\cos\lambda_1 l - \cosh\lambda_2 l}{\frac{\lambda_2}{\lambda_1}\sin\lambda_1 l - \sinh\lambda_2 l}$

If the contributions of vertical stress σ_{zz}, surface stress τ_{nx}, surface density ρ_0 and surface stresses on the vertical sides of a rectangular beam are neglected, then equation (3.1) reduces to the governing equation proposed by Gurtin et al. [39] as following,

$$[EI + (2\mu_0 + \lambda_0)I^{**}]\frac{\partial^4 w}{\partial x^4} + \rho A\frac{\partial^2 w}{\partial t^2} + q(x) = 0 \tag{3.9}$$

$I^{**} = 2bh^2$ is simplified perimeter moment of inertia for a rectangular cross-section with height $2h$ and width b. Comparing equation (3.9) to the classical governing equation for thin beam vibration, it can be seen that the only difference between the classical case and the simplified surface energy incorporated beam model is the modified bending stiffness. Therefore, the natural frequency of a cantilever beam governed by equation (3.9) can be written in terms of classical natural frequency f_{class} in the following form,

$$f^2 = f_{class}^2\left[1 + \frac{(2\mu_0 + \lambda_0)I^{**}}{EI}\right] \tag{3.10}$$

For a beam of rectangular cross section of height H, equation (3.10) can be rewritten as $f^2 = f_{class}^2\left[1+\frac{6(2\mu_0+\lambda_0)}{EH}\right]$, which is identical to the solution given by Gurtin and coworkers [19, 39].

3.1.2 Thick Beam Free Vibration

The equations of motion for thick beam free vibration can be written as,

$$G\kappa A(\frac{\partial^2 w}{\partial x^2}+\frac{\partial \phi}{\partial x})+\tau_0 s^*\frac{\partial^2 w}{\partial x^2}=(\rho A+\rho_0 s^*)\frac{\partial^2 w}{\partial t^2} \tag{3.11}$$

$$[EI+(2\mu_0+\lambda_0)I^*]\frac{\partial^2\phi}{\partial x^2}+\frac{2\nu I\tau_0}{H}\frac{\partial^3 w}{\partial x^3}-G\kappa A(\frac{\partial w}{\partial x}+\phi)$$

$$=(\rho I+\rho_0 I^*)\frac{\partial^2\phi}{\partial t^2}+I^0\frac{\partial^3 w}{\partial x\partial t^2} \tag{3.12}$$

To obtain the characteristic equations of transverse vibration, it is assumed that the transverse and angular displacements are in the following forms respectively,

$$w=W(x)\sin\omega t\,;\ \phi=\psi(x)\sin\omega t \tag{3.13}$$

where ω is the natural frequency, $W(x)$ and $\psi(x)$ are vibration modes of the transverse and angular displacements respectively.

Substitution of equation (3.13) into (3.11) and (3.12) and the solution of the resulting pair of coupled ordinary differential equations yield,

$$W(x)=C_1\sin\gamma_1 x+C_2\cos\gamma_1 x+C_3\sinh\gamma_2 x+C_4\cosh\gamma_2 x \tag{3.14}$$

$$\psi(x)=C_1k_a\cos\gamma_1 x-C_2k_a\sin\gamma_1 x+C_3k_b\cosh\gamma_2 x+C_4k_b\sinh\gamma_2 x \tag{3.15}$$

where C_1 to C_4 are four arbitrary unknowns.

$$\gamma_1=\left(\frac{\Lambda_1+\sqrt{\Lambda_1^2-4\Lambda_2}}{2}\right)^{1/2};\gamma_2=\left(\frac{-\Lambda_1+\sqrt{\Lambda_1^2-4\Lambda_2}}{2}\right)^{1/2}$$

$$\Lambda_1=\frac{[EI+(2\mu_0+\lambda_0)I^*]M^*\omega^2/G\kappa A+(1+\tau_0 s^*/G\kappa A)(\rho I+\rho_0 I^*)\omega^2-I^0\omega^2-\tau_0 s^*}{K_s}$$

$$\Lambda_2=\frac{(\rho I+\rho_0 I^*)M^*\omega^4/G\kappa A-M^*\omega^2}{K_s}$$

$$k_a = -(1+\frac{\tau_0 s^*}{G\kappa A})\gamma_1 + (\frac{M^*\omega^2}{G\kappa A})\frac{1}{\gamma_1}$$

$$k_b = -(1+\frac{\tau_0 s^*}{G\kappa A})\gamma_2 - (\frac{M^*\omega^2}{G\kappa A})\frac{1}{\gamma_2} \tag{3.16}$$

Note that if the surface quantities are all neglected, the above general solutions are reduced to the classical solutions given by Huang [55].

By substituting above general solutions into the boundary conditions, the characteristic equations for different types of thick beams are obtained as following,

Simply Supported (SS) Beams

The boundary conditions are given in equation (2.32). By substituting equations (3.14) and (3.15) into the boundary conditions, the characteristic equation for natural frequencies can be obtained as,

$$\sin\gamma_1 L \sinh\gamma_2 L = 0 \tag{3.17}$$

Cantilever (C) Beams

For a cantilever thick beam, the characteristic equation can be derived as,

$$\begin{aligned} &-B_3B_4k_a + B_1B_2k_b + (B_1B_4k_b + B_3B_2k_a)\sin\gamma_1 L \sinh\gamma_2 L \\ &\quad +(B_3B_2k_b - B_1B_4k_a)\cos\gamma_1 L \cosh\gamma_2 L = 0 \end{aligned} \tag{3.18}$$

where $B_1 = \left[EI + (2\mu_0 + \lambda_0)I^*\right]\gamma_1 k_a + \dfrac{2\nu I\tau_0}{H}\gamma_1^2 - I^0\omega^2$

$$B_2 = (G\kappa A + \tau_0 s^*)\gamma_1 + G\kappa A k_a$$

$$B_3 = [EI + (2\mu_0 + \lambda_0)I^*]\gamma_2 k_a + \frac{2\nu I\tau_0}{H}\gamma_2^2 + I^0\omega^2$$

$$B_4 = (G\kappa A + \tau_0 s^*)\gamma_2 + G\kappa A k_b \tag{3.19}$$

Clamped-Clamped (CC) Beam

For a clamped-clamped beam, the characteristic equation is obtained as,

$$(k_a^2 - k_b^2)\sin\gamma_1 L \sinh\gamma_2 L + 2k_a k_b(\cos\gamma_1 L \cosh\gamma_2 L - 1) = 0 \tag{3.20}$$

3.1.3 Numerical Results

By solving the characteristic equations derived in the last two subsections, the natural frequencies of thin and thick Al and Si beams were computed. In the calculations, the dimensions for thin beams are $L = 120nm$, $H = 2h = 6nm$ and $b = 3nm$, and those for thick beams are $L = 50nm$, $H = 2h = 6nm$ and $b = 3nm$. The solutions are shown in Tables 3.2 and 3.3. The corresponding solutions from classical thin and thick beam theories are also presented in parenthesis. It is found that surface energy effects have a significant influence on the first natural frequency of thin and thick beams for the three common boundary conditions considered in this study. The highest influence is observed for cantilever beams followed by SS and CC beams. However, the higher natural frequencies are not significantly affected as the bulk bending stiffness becomes the dominant factor controlling the higher modes. It is worth pointing out that the natural frequencies with surface effects could increase or decrease compared with the classical results, depending on the signs of the surface elastic constants, wave number and also the boundary conditions. Take the Si thin simply-supported beam for example, the natural frequencies are shown as $\omega_{ns}^2 = \dfrac{(EI + (2\mu_0 + \lambda_0)I^* - \dfrac{2\nu I\tau_0}{H})(\dfrac{n\pi}{L})^4 + \tau_0(\dfrac{n\pi}{L})^2}{\rho A}$ (the surface density ρ_0 is so small that its effect is neglected in the expression). The classical natural frequencies for simply-supported beam can be written as $\omega_n^2 = \dfrac{EI(\dfrac{n\pi}{L})^4}{\rho A}$. Therefore the non-dimensional difference is derived as,

$$\frac{\omega_{ns}^2 - \omega_n^2}{\omega_n^2} = \frac{[(2\mu_0 + \lambda_0)I^* - \dfrac{2\nu I\tau_0}{H}] + \tau_0(\dfrac{L}{n\pi})^2}{EI} \tag{3.21}$$

In the case of Si, $(2\mu_0 + \lambda_0)I^* - \dfrac{2\nu I\tau_0}{H}$ is negative, and $\tau_0(\dfrac{L}{n\pi})^2$ is positive. When the wave number n is small, the summation of the two terms in the numerator of equation (3.21) is positive, therefore the frequency from surface elastic model is higher than classical result. While the value of $\tau_0(\dfrac{L}{n\pi})^2$ will decrease with increasing wave number, thus the first term of the numerator in equation (3.21) will become dominant after the wave number reaches certain integer. As a result, for higher natural frequencies, the results from surface elastic model become smaller compared to the classical ones. This trend can be observed from Tables 3.2 and 3.3. In fact for some higher modes, the classical solution overestimates the natural frequencies by 2-8%. It should be noted that thin beam theory is not generally accurate for higher modes and the thick beam theory should be used irrespective of the L/H ratio. The mode shapes of SS, C and CC beams were also compared. It is found that the mode shapes with surface energy effects are identical to the classical mode shapes for the SS and CC beams. A noticeable difference is observed for a cantilever beam and the corresponding mode shapes of a cantilevered Al beam are shown in Figure 3.1.

Table 3.2 Natural frequencies of aluminum beams

Beam type	1st (GHz)	2nd(GHz)	3rd (GHz)	4th (GHz)
Thin SS	1.45 (1.09)	4.47 (4.36)	9.39 (9.82)	16.27 (17.45)
Thin C	0.75 (0.39)	2.90 (2.44)	6.82 (6.82)	12.69 (13.36)
Thin CC	2.52 (2.47)	6.37 (6.82)	12.49 (13.36)	20.35 (22.09)
Thick SS	6.10 (6.14)	21.49(23.13)	43.96 (47.84)	71.08 (77.43)
Thick C	2.62 (2.21)	12.60(13.05)	31.24 (33.74)	55.31 (60.16)
Thick CC	12.18(13.05)	30.40(32.79)	53.92 (58.25)	80.85(87.12)

Natural frequency from the corresponding classical theory is shown in parenthesis.

Table 3.3 Natural frequencies of silicon beams

Beam type	1st (GHz)	2nd(GHz)	3rd (GHz)	4th (GHz)
Thin SS	1.66 (1.28)	5.19 (5.12)	10.96 (11.53)	19.02 (20.49)
Thin C	0.86 (0.46)	3.34 (2.86)	7.93 (8.01)	14.81 (15.69)
Thin CC	2.94 (2.90)	7.64 (8.00)	14.59 (15.69)	23.83 (25.93)
Thick SS	7.08 (7.20)	25.07(27.02)	51.33 (55.70)	82.92 (89.76)
Thick C	3.02 (2.60)	14.67(15.28)	36.48 (39.31)	64.46 (69.74)
Thick CC	14.20(15.25)	35.41(38.10)	62.74 (67.38)	93.86(100.47)

Natural frequency from the corresponding classical theory is shown in parenthesis.

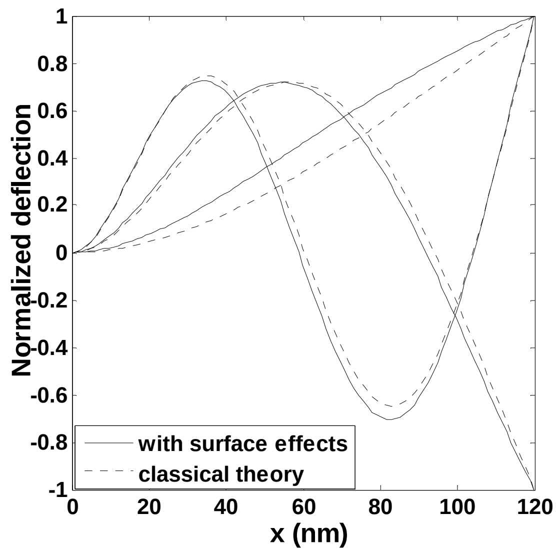

Figure 3.1 Comparison of mode shapes of a cantilevered Al beam based on thin beam model and classical theory.

3.2 Study on Natural Frequency of GaAs Cantilever

Previous section has shown the substantial influence of surface energy effects on the natural frequencies of the nanoscale beams. This has also been observed in many experimental works, among which, Lagowski and his coworkers [38] reported that the measured natural frequencies of GaAs cantilever beams are noticeably below those predicted by classical beam theory. Especially when the dimensions become small, the first natural frequency does not follow the linear variation with respect to H/L^2 ratio as expected from classical theory. Instead, they increase with decreasing values of H/L^2. This phenomenon has been discussed in [38, 39]. Gurtin concludes that surface residual stress does not influence the first natural frequency while surface elasticity can within linear theory of elasticity. In the following, we revisit these experimental data. The first natural frequency of a cantilever beam with surface elastic terms needs to be determined. The characteristic equation to determine the natural frequencies has been presented in Section 3.1. A closed-form analytical solution remains a challenge. Therefore, we need to adopt energy method to obtain the closed-form solution for the first natural frequency.

We follow Rayleigh's energy method with surface elastic terms included to fit the experimental data of GaAs cantilever beams reported by Lagowski. A closed-form expression for the first natural frequency as a function of surface elastic material constants allows us to determine their values.

Lord Rayleigh pioneered an energy method that can be used to estimate natural frequencies or buckling loads (eigenvalues in general) of linear elastic structures by suitably choosing displacement functions (guessing eigenvectors) that satisfy kinematic boundary conditions. To this end, a quotient, called Rayleigh quotient, is defined as the ratio of potential and kinetic energies in vibration problems. Similar quotient can be defined for buckling problems too. A fundamental property of Rayleigh quotient is its stationarity with respect to small perturbations in displacement functions. Consequently, even if one makes errors in the choice of displacement function, say of the order ε, the error introduced in the natural frequency estimate is of second order ε^2. Hence, a Rayleigh quotient can be used to obtain the fundamental natural frequency very accurately.

As the system is conservative, strain energy stored in the bulk can be written as,

$$
\begin{aligned}
U^B &= \frac{1}{2}\int_V \sigma_{xx}\varepsilon_{xx}\,dV \\
&= \frac{1}{2}\int_V \left(-Ez\frac{d^2w}{dx} + \frac{2\nu\tau_0 z}{H}\frac{\partial^2 w}{\partial x^2}\right)\left(-z\frac{d^2w}{dx}\right)dV \\
&= \frac{1}{2}\left(EI - \frac{2\nu I\tau_0}{H}\right)\int_0^l \left(\frac{d^2w}{dx^2}\right)^2 dx \qquad (3.22)
\end{aligned}
$$

The strain energy stored in the surface can be written as,

$$
\begin{aligned}
U^s &= \frac{1}{2}\int_\Gamma (\tau_{xx}\varepsilon_{xx} + \tau_{nx}\varepsilon_{nx})\,d\Gamma \\
&= \frac{1}{2}\int_\Gamma \left[\left(\tau_0 - z(2\mu_0+\lambda_0)\frac{d^2w}{dx^2}\right)\left(-z\frac{d^2w}{dx}\right) + \left(\tau_0\frac{dw}{dx}n_z\right)\left(\frac{dw}{dx}n_z\right)\right]d\Gamma \\
&= \frac{1}{2}(2\mu_0+\lambda_0)I^*\int_0^l \left(\frac{d^2w}{dx^2}\right)^2 dx + \frac{1}{2}\tau_0 s^*\int_0^l \left(\frac{dw}{dx}\right)^2 dx \qquad (3.23)
\end{aligned}
$$

where V is the bulk volume, Γ is the surface area. The stresses and strains for the bulk and surface can be found in Chapter 2. Therefore the total energy is derived as,

$$
\begin{aligned}
U &= U^B + U^s \\
&= \frac{1}{2}\left(EI + (2\mu_0+\lambda_0)I^* - \frac{2\nu I\tau_0}{H}\right)\int_0^l \left(\frac{\partial^2 w}{\partial x^2}\right)^2 dx + \frac{1}{2}\tau_0 s^*\int_0^l \left(\frac{\partial w}{\partial x}\right)^2 dx \qquad (3.24)
\end{aligned}
$$

The kinetic energy T stored in the overall system is shown as,

$$T = T^B + T^s$$
$$= \frac{1}{2}\int_0^l \rho A(\dot{w})^2 dx + \frac{1}{2}\int_0^l \rho_0 s^* (\dot{w})^2 dx \tag{3.25}$$

The principle of conservation of energy requires that,

$$U_{\max} = T_{\max} \tag{3.26}$$

For free vibration, the transverse deflection can be expressed as,

$$w(x,t) = W_n(x)\sin\omega_n t \tag{3.27}$$

Substitution of equation (3.27) into equations (3.24)-(3.26) yields,

$$\omega_n^2 = \frac{K_b \int_0^l (W_n''(x))^2 dx + \tau_0 s^* \int_0^l (W_n'(x))^2 dx}{M^* \int_0^l (W_n(x))^2 dx} \tag{3.28}$$

where $K_b = EI + (2\mu_0 + \lambda_0)I^* - \dfrac{2\nu I \tau_0}{H}$ and $M^* = (\rho A + \rho_0 s^*)$. Equation (3.28) is in the form of Rayleigh quotient [56]. $W_n(x)$ is a suitable mode shape of vibration, which is not known in advance. A suitable candidate for $W_n(x)$ is the function that is sufficiently differentiable as required in equation (3.28) and satisfies the geometric boundary conditions of the problem.

For a simply supported beam, it has been found in Section 3.1 that the first mode shape with surface effects is identical to the classical one, which is known as,

$$W_n(x) = \sin\frac{n\pi}{L}x \tag{3.29}$$

Substitution of above shape function into equation (3.28) yields the natural frequencies of simply supported beam as,

$$\omega_n^2 = \frac{K_b(\frac{n\pi}{L})^4 + \tau_0 s^*(\frac{n\pi}{L})^2}{M^*} \tag{3.30}$$

The solution using energy method in equation (3.30) is identical to that shown in equation (3.6) except for an additional term $I^0 = \dfrac{2\nu I \rho_0}{H}$ in equation (3.6). This is due to the consideration of vertical stress σ_{zz} in our previous formulation. It has been proved numerically that σ_{zz} is trivial and can be neglected in all practical cases. Therefore it can be seen that the solution estimated by the Rayleigh quotient is very accurate.

Based on above verification, we can further apply this method confidently to determine the natural frequency of a cantilever beam. As the influence of vertical stress σ_{zz} and the surface density ρ_0 are shown numerically to be very small on the dynamic response of beams, they can be neglected for the sake of simplicity. Thus, the natural frequencies in equation (3.28) can be simplified as,

$$\omega_n^2 = \frac{(EI + (2\mu_0 + \lambda_0)I^*)\int_0^l (W_n''(x))^2 dx + \tau_0 s^* \int_0^l (W_n'(x))^2 dx}{\rho A \int_0^l (W_n(x))^2 dx} \tag{3.31}$$

Non-dimensional quantities, $\bar{x} = x / L$, $\bar{W}_n(\bar{x}) = W_n(\bar{x}) / L$ are introduced; rewrite equation (3.31) as,

$$\omega_n^2 = \frac{(EI + (2\mu_0 + \lambda_0)I^*)\int_0^1 (\bar{W}_n''(\bar{x}))^2 d\bar{x} + \tau_0 s^* L^2 \int_0^1 (\bar{W}_n'(\bar{x}))^2 d\bar{x}}{\rho A L^4 \int_0^1 (\bar{W}_n(\bar{x}))^2 d\bar{x}}$$

$$= \frac{(EI + (2\mu_0 + \lambda_0)I^*)A_n + \tau_0 s^* L^2 B_n}{\rho A L^4 C_n} \tag{3.32}$$

where $A_n = \int_0^1 (\bar{W}_n''(\bar{x}))^2 d\bar{x}$

$B_n = \int_0^1 (\bar{W}_n'(\bar{x}))^2 d\bar{x}$

$$C_n = \int_0^1 (\bar{W}_n(\bar{x}))^2 d\bar{x}\,. \tag{3.33}$$

Rewrite equation (3.32) as a function of H / L^2 for a rectangular cross-section as,

$$\omega_n^2 = \frac{A_n}{C_n \rho}\left(\frac{E}{12} + \frac{(2\mu_0 + \lambda_0)}{6b}\right)\left(\frac{H}{L^2}\right)^2 + \frac{A_n(2\mu_0 + \lambda_0)}{2C_n \rho L^2}\left(\frac{H}{L^2}\right) + \frac{2\tau_0 B_n}{C_n \rho L^4}\left(\frac{L^2}{H}\right)$$

$$= D_n X^2 + E_n X + \frac{F_n}{X} \tag{3.34}$$

where $X = H / L^2$, $D_n = \frac{A_n}{C_n \rho}\left(\frac{E}{12} + \frac{(2\mu_0 + \lambda_0)}{6b}\right)$, $E_n = \frac{A_n(2\mu_0 + \lambda_0)}{2C_n \rho L^2}$ and $F_n = \frac{2\tau_0 B_n}{C_n \rho L^4}$.

From equation (3.34), the fundamental natural frequency of cantilever beam can be obtained as,

$$\omega_1^2 = D_1 X^2 + E_1 X + \frac{F_1}{X} \tag{3.35}$$

where $D_1 = \frac{A_1}{C_1 \rho} \left(\frac{E}{12} + \frac{(2\mu_0 + \lambda_0)}{6b} \right)$

$$E_1 = \frac{A_1 (2\mu_0 + \lambda_0)}{2 C_1 \rho L^2}$$

$$F_1 = \frac{2\tau_0 B_1}{C_1 \rho L^4} \tag{3.36}$$

With equation (3.35), we are able to examine the experimental data reported by Lagowski et al. [38]. In their experiments, the fundamental natural frequencies of GaAs wafer in the configuration of cantilevers whose dimensions range from 3 to 50 μm in thickness, 6 to 15 mm in length, and 1 to 1.5 mm in width are measured. It can be seen in Figure 3.2 that the experimental data show a unique trend that the classical theory cannot emulate. Equation (3.35) is applied to fit the experimental data using least square fit. Our surface elasticity model can successfully capture the experimental trend as shown in Figure 3.2. The least squares fit yields the values of the parameters D_1, E_1 and F_1 as 3.6415×10^7, -1.196×10^7 and 0.0204×10^7 respectively.

With a good guess of eigenfuction $W_1(x)$ for cantilever fundamental mode shape, the values of Young's modulus for the bulk, the surface elastic properties as well as the surface residual stress can be determined. As mentioned earlier, suitable guess of $W_n(x)$ is the function that is sufficiently differentiable and satisfies the geometric boundary conditions of the problem. Good approximations can be the deflection of the beam under its own weight or first buckling mode. In the present study, the first buckling mode is used as an approximation given as,

$$\bar{W}_1(x) = \cos \frac{\pi \bar{x}}{2} - 1 \tag{3.37}$$

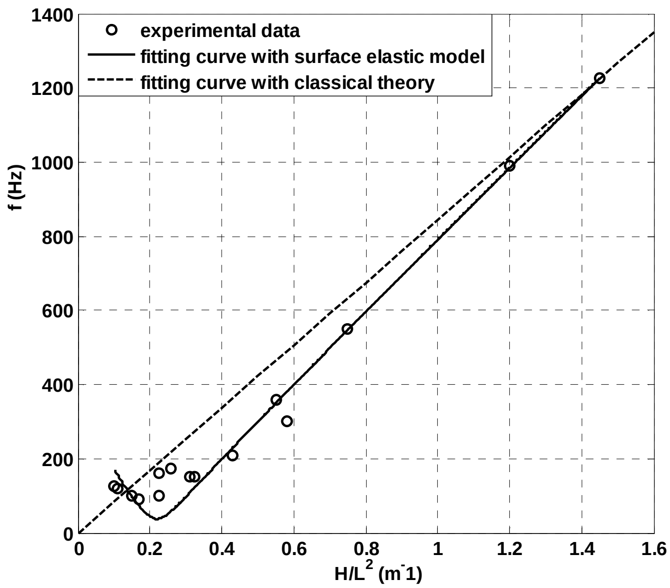

Figure 3.2 Natural frequency of vibration of thin (111) GaAs crystals in cantilever configuration as a function of crystal dimensions H/L^2

Substitution of equation (3.37) into equation (3.33) yields $A_1 = \frac{\pi^4}{32}$, $B_1 = \frac{\pi^2}{8}$ and $C_1 = \frac{3}{2} - \frac{4}{\pi}$. Solving equation (3.36) using above obtained values yields the material properties of GaAs as, $\tau_0 = 0.9968 N/m$, $2\mu_0 + \lambda_0 = -9.4743\times10^5 N/m$, $E = 174.97 Gpa$. Compared with the Young's modulus of GaAs used in the experiment $E = 131.15 Gpa$, the prediction using our model provides reasonably good results. Note that the value of Young's modulus used in the experiment is determined by fitting the first natural frequencies in the classical formulation. The natural frequencies measured in the experiment are of specimens with different dimensions under room pressure. As the accuracy of measurement is influenced by factors, such as ambient atmosphere, damping and specimen geometry, so the value presented is just an approximation to the real case. The dimensions of the cantilever beam are not explicitly given, thus $L = 10mm$ and $b = 1mm$ are used in the calculation. It is shown that varying b in the given range has unnoticeable effects on the values of all material constants. Varying the values of L

gives noticeable changes in surface properties, but negligible change in Young's modulus.

A review of equation (3.35) along with the above obtained material constants can well explain the trend in the experiment. The difference between the natural frequencies obtained from experiments and classical theory is attributed to two parts, surface elastic constants $2\mu_0 + \lambda_0$ present in the first two terms of equation (3.35) and surface residual stress τ_0 in the last term of equation (3.35). The overall effects from the surface depend on the combination of the two parameters. For GaAs, $2\mu_0 + \lambda_0$ is negative so that it will decrease the natural frequency. While τ_0 is positive, thus it will increase the natural frequency. At large H/L^2, $2\mu_0 + \lambda_0$ plays dominant role; therefore smaller natural frequencies compared to classical predictions are observed. When H/L^2 goes small, the effect of τ_0 will surpass that of $2\mu_0 + \lambda_0$; as a result the natural frequencies are increased compared to the classical ones. The reason for increasing natural frequency with decreasing H/L^2 is entirely due to the presence of last term in equation (3.35).

3.3 Influence of Surface Residual Stress

Analyses in Chapter 2 and 3 indicate that the surface elasticity modifies the bending stiffness of nanoscale beams, which consequently influences their static and dynamic response. This agrees well with the existing literature [16, 22, 44]. The surface residual stress is also found to influence mechanical behaviour of nanoscale beams and the effects are shown to be significant in our numerical study.

The effect of surface residual stress has been debated extensively. Lagowski and his coworkers [38] idealised the surface residual stress as compressive force acting on a typical beam element in the bulk. They reported that the surface residual stress affects the first natural frequency. This was later shown to be incorrect by Gurtin et al. [39]. They showed that the transverse distributed load arising due to Young-Laplace relation cancels the force term associated with compressive force in the beam bending equation derived by Lagowski et al. However, Gurtin did not consider all the surfaces. Moreover, both the approaches are in violation of Newton's third law: there is no externally applied compressive force that can balance the axial stress resultant of a bulk element at either ends of the beam. In our one-dimensional beam model we avoid this by ensuring that there is no net axial force acting on a cross section. We found that the surface residual stress does influence the first natural frequency. Our approximate engineering beam model is consistent with the results of Wang et al. [31]. They presented a rigorous 3-D elasticity model to investigate the effects of surface elasticity and surface residual stress on the elastic properties of nanoscale structures. They found that besides surface elasticity, the surface residual stress also affects the effective Young's modulus of nanoscale structures. Thus the first natural frequency is influenced by surface residual stress in our model and that of Wang et al. [31].

Chapter 4

FINITE ELEMENT ANALYSIS OF NANOSCALE BEAMS

4.1 Finite Element Formulation

Analytical models can be used for simple geometries and boundary conditions. For the analysis of complex geometries and boundary conditions such as those encountered in NEMS and other nanotechnology applications, versatile numerical models such as the finite element method (FEM) need to be developed. The conventional FEM cannot characterize the size-dependent behavior. In this chapter, new finite element models based on the beam theories presented in Chapters 2 and 3 are developed to incorporate the surface effects into the classical FEM. A detailed derivation of the finite element formulation by using Galerkin's method is presented. Thereafter, the finite element scheme is applied to study static and dynamic response of thin and thick beam under different loading and boundary conditions. A comparison with the analytical solutions given in Chapter 2 and 3 is also presented to confirm the accuracy and convergence of the finite element solutions.

4.1.1 Thin Beam Static Bending

For thin beams under a static transverse loading and an axial compression, the governing equation of thin beams has been derived in Section 2.4 as shown in equation (2.59) as,

$$[EI+(2\mu_0+\lambda_0)I^*-\frac{2\nu I\tau_0}{H}]\frac{\partial^4 w}{\partial x^4}+(F-\tau_0 s^*)\frac{\partial^2 w}{\partial x^2}+q(x)=0 \qquad (4.1)$$

One of the weighted residual methods, Galerkin's method, is applied to develop the finite element formulation and the corresponding matrix equations.

The weighted residual statement of equation (4.1) can be written as,

$$\psi=\int_0^L\left\{[EI+(2\mu_0+\lambda_0)I^*-\frac{2\nu I\tau_0}{H}]\frac{d^4 w}{dx^4}+(F-\tau_0 s^*)\frac{d^2 w}{dx^2}+q(x)\right\}\bar{w}dx=0 \qquad (4.2)$$

where L is the length of the beam and $\bar{w}$ is the weighting function. Integrating equation (4.2) by part, the weak formulation of equation (4.2) is obtained as,

$$\psi = \int_0^L \left\{ [EI + (2\mu_0 + \lambda_0)I^* - \frac{2\nu I\tau_0}{H}] \frac{d^2 w}{dx^2} \frac{d^2 \bar{w}}{dx^2} - (F - \tau_0 s^*) \frac{dw}{dx} \frac{d\bar{w}}{dx} + q\bar{w} \right\} dx$$

$$+ (M \frac{d\bar{w}}{dx} - Q\bar{w}) \bigg|_0^L = 0 \quad (4.3)$$

where $M = -[EI + (2\mu_0 + \lambda_0)I^* - \frac{2\nu I\tau_0}{H}] \frac{d^2 w}{dx^2}$ and $Q = -[EI + (2\mu_0 + \lambda_0)I^* - \frac{2\nu I\tau_0}{H}] \frac{d^3 w}{dx^3} - (F - \tau_0 s^*) \frac{dw}{dx}$ are the bending moment and shear force respectively.

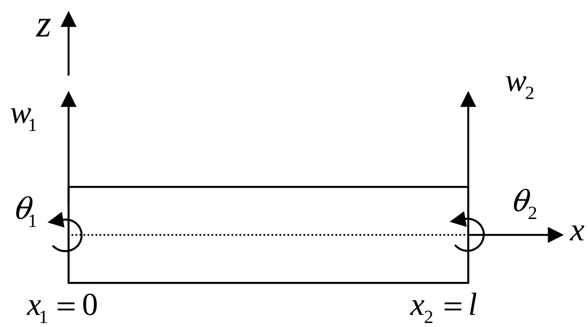

Figure 4.1 Two node beam element for thin beam

Consider a 2-node finite element with two nodal degrees of freedom per node, i.e., w and $\theta = \frac{dw}{dx}$, as shown in Figure 4.1. The element nodal displacement vector is,

$$w^e = \begin{bmatrix} w_1 & \theta_1 & w_2 & \theta_2 \end{bmatrix} \quad (4.4)$$

The transverse displacement w is interpolated by using Hermitian shape functions as,

$$w = N(x)w^e \quad (4.5)$$

where the shape functions are given as,

$$N_1(x) = 1 - \frac{3x^2}{l^2} + \frac{2x^3}{l^3}, \quad N_2(x) = x - \frac{2x^2}{l} + \frac{x^3}{l^2}$$

$$N_3(x) = \frac{3x^2}{l^2} - \frac{2x^3}{l^3}, \quad N_4(x) = -\frac{x^2}{l} + \frac{x^3}{l^2} \quad (4.6)$$

Substitution of equation (4.5) into equation (4.3) yields,

$$\int_0^l \left\{ [EI + (2\mu_0 + \lambda_0)I^* - \frac{2\nu I\tau_0}{H}] N''^T N'' - FN'^T N' + \tau_0 s^* N'^T N' \right\} w^e dx = -\int_0^l q(x) N dx \quad (4.7)$$

Therefore, the element stiffness matrix is obtained as,

$$\left[K^e\right]=\int_0^l\left\{[EI+(2\mu_0+\lambda_0)I^*-\frac{2\nu I\tau_0}{H}]N''^T N''-FN'^T N'+\tau_0 s^* N'^T N'\right\}dx$$

$$=\frac{[EI+(2\mu_0+\lambda_0)I^*-\frac{2\nu I\tau_0}{H}]}{l^3}\begin{bmatrix}12 & 6l & -12 & 6l\\ 6l & 4l^2 & -6l & 2l^2\\ -12 & -6l & 12 & -6l\\ 6l & 2l^2 & -6l & 4l^2\end{bmatrix}$$

$$-\frac{(F-\tau_0 s^*)}{30l}\begin{bmatrix}36 & 3l & -36 & 3l\\ 3l & 4l^2 & -3l & -l^2\\ -36 & -3l & 36 & -3l\\ 3l & -l^2 & -3l & 4l^2\end{bmatrix} \tag{4.8}$$

The element force vector is defined as,

$$\left\{R^e\right\}=-\int_0^l q(x)Ndx \tag{4.9}$$

If the element is subjected to a uniform pressure q_0, the force vector becomes

$$\left\{R^e\right\}=-\frac{q_0}{12}\left[6l \quad l^2 \quad 6l \quad -l^2\right]^T \tag{4.10}$$

In the case of concentrated force within the beam element, the force vector is

$$\left\{R^e\right\}=\int_0^l -P\delta(x-x_0)Ndx$$

$$=-P\left[N_1(x_0) \quad N_2(x_0) \quad N_3(x_0) \quad N_4(x_0)\right]^T \tag{4.11}$$

where P is the concentrated force applied at point $x=x_0$.

The assembly of element stiffness matrices and nodal force vectors yield the global equilibrium equations as,

$$\left[K\right]\left\{r\right\}=\left\{R\right\} \tag{4.12}$$

where $\left[K\right]$ is the global stiffness matrix and $\left\{R\right\}$ is the global force vector.

4.1.2 Thin Beam Free Vibration

For dynamic analysis, the inertial forces on the right hand side of thin beam governing equation (2.23) are included in the finite element formulation and these terms correspond to the element mass matrix. The transverse deflection is a function of x and t. The deflection is interpolated within the beam element as,

$$w(x,t) = N(x)w^e(t) \tag{4.13}$$

The same interpolation functions are used to obtain a 'consistent' mass matrix. Substitution of equation (4.13) into the inertial force terms yields,

$$\int_0^l \left\{ (\rho A + \rho_0 s^*) N^T N - \frac{2\nu I \rho_0}{H} N'^T N' \right\} \ddot{w}^e(t) dx \tag{4.14}$$

where superimposed dot denotes temporal derivative. From equation (4.14), the element mass matrix becomes,

$$\begin{aligned} \left[m^e \right] &= \int_0^l \left\{ (\rho A + \rho_0 s^*) N^T N - \frac{2\nu I \rho_0}{H} N'^T N' \right\} dx \\ &= \frac{(\rho A + \rho_0 s^*) l}{420} \begin{bmatrix} 156 & 22l & 54 & -13l \\ 22l & 4l^2 & 13l & -3l^2 \\ 54 & 13l & 156 & -22l \\ -13l & -3l^2 & -22l & 3l \end{bmatrix} - \frac{\nu I \rho_0}{15Hl} \begin{bmatrix} 36 & 3l & -36 & 3l \\ 3l & 4l^2 & -3l & -l^2 \\ -36 & -3l & 36 & -3l \\ 3l & -l^2 & -3l & 4l^2 \end{bmatrix} \end{aligned} \tag{4.15}$$

Thus, the global matrix equation for dynamic beam analysis is obtained after assembly of element matrices and vectors,

$$[M]\{\ddot{r}\} + [K]\{r\} = \{R(t)\} \tag{4.16}$$

where $[M]$ is the global mass matrix. In the case of free vibration problems, $w^e(t) = e^{i\omega t} w^e$, it becomes an eigenvalue problem,

$$([K] - \omega^2 [M])\{r\} = 0 \tag{4.17}$$

where ω is the angular frequency of vibration in rad/s. $\{r\}$ is the mode shape.

4.1.3 Thick Beam Static Bending

In the case of thick beams under static transverse loading and uniaxial compressive force, a term $-F\dfrac{dw}{dx}$ corresponding to the presence of compressive force needs to be added to the moment equilibrium of equation (2.19). Therefore, the governing equations for thick beam are modified as,

$$G\kappa A(\frac{\partial^2 w}{\partial x^2}+\frac{\partial \phi}{\partial x})+\tau_0 s^*\frac{\partial^2 w}{\partial x^2}-q(x)=(\rho A+\rho_0 s^*)\frac{\partial^2 w}{\partial t^2} \tag{4.17}$$

$$[EI+(2\mu_0+\lambda_0)I^*]\frac{\partial^2 \phi}{\partial x^2}+\frac{2\nu I\tau_0}{H}\frac{\partial^3 w}{\partial x^3}-F\frac{\partial w}{\partial x}-G\kappa A(\frac{\partial w}{\partial x}+\phi)$$
$$=(\rho I+\rho_0 I^*)\frac{\partial^2 \phi}{\partial t^2}+\frac{2\nu I\rho_0}{H}\frac{\partial^3 w}{\partial x\partial t^2} \tag{4.18}$$

In the same procedure, applying Galerkin's method again leads to the following weighted residual statement.

$$\psi=\int_0^L\{(G\kappa A(\frac{d^2 w}{dx^2}+\frac{d\phi}{dx})+\tau_0 s^*\frac{d^2 w}{dx^2}-q(x))\bar{w}$$
$$+([EI+(2\mu_0+\lambda_0)I^*]\frac{d^2\phi}{dx^2}+\frac{2\nu I\tau_0}{H}\frac{d^3 w}{dx^3}-F\frac{dw}{dx}-G\kappa A(\frac{dw}{dx}+\phi))\bar{\phi}\}dx=0 \tag{4.19}$$

where $\begin{Bmatrix}\bar{w}\\ \bar{\phi}\end{Bmatrix}$ is the weight function.

Integrating equation (4.19) by part yields the week formulation as,

$$\int_0^L\{G\kappa A(\frac{dw}{dx}+\phi)(\frac{d\bar{w}}{dx}+\bar{\phi})+[EI+(2\mu_0+\lambda_0)I^*]\frac{d\phi}{dx}\frac{d\bar{\phi}}{dx}$$
$$+\frac{2\nu I\tau_0}{H}\frac{d^2 w}{dx^2}\frac{d\bar{\phi}}{dx}+F\frac{dw}{dx}\bar{\phi}+\tau_0 s^*\frac{dw}{dx}\frac{d\bar{w}}{dx}+q(x)\bar{w}\}dx-(Q\bar{w}+M\bar{\phi})\Big|_0^L=0 \tag{4.20}$$

To derive the stiffness matrix for a thick beam, the element generalized displacements w and ϕ need to be interpolated within each element. As the transverse deflection w and the angular displacement ϕ are independent variables for a thick beam, they can be interpolated independently using proper shape functions. Due to the presence of second derivative of w in the equation (4.20), C^0 continuous shape functions which are normally used in classical thick beam cannot be applied in the present case. To satisfy the continuity between the neighboring elements, C^1 shape functions can be used for the new thick beam element. As a result, a 3-node beam element with two degrees of freedom per node (w and ϕ) shown in Figure 4.2 is used for both variables in this study.

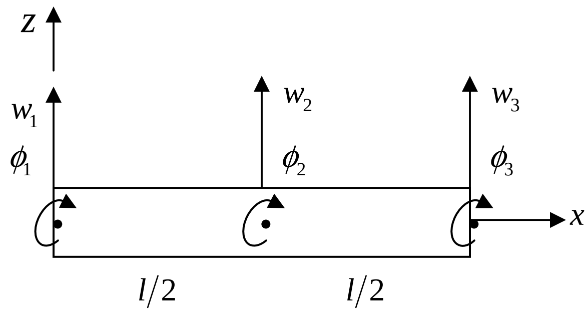

Figure 4.2 Three node beam element for thick beam

The displacements are interpolated as,

$$\begin{Bmatrix} w \\ \phi \end{Bmatrix} = \begin{bmatrix} N_1 & 0 & N_2 & 0 & N_3 & 0 \\ 0 & N_1 & 0 & N_2 & 0 & N_3 \end{bmatrix} \begin{Bmatrix} w_1 \\ \phi_1 \\ w_2 \\ \phi_2 \\ w_3 \\ \phi_3 \end{Bmatrix} \tag{4.21}$$

where $N_i (i = 1, 2, 3)$ are shape functions given as,

$$N_1 = \frac{2x^2}{l^2} - \frac{3x}{l} + 1$$

$$N_2 = -\frac{4x^2}{l^2} + \frac{4x}{l}$$

$$N_3 = \frac{2x^2}{l^2} - \frac{x}{l}\,. \tag{4.22}$$

Using equation (4.22) and (4.21) along with equation (4.20) yields the following stiffness matrix for thick beam.

$$\left[K^e\right] = \left[K_1^e\right] + \left[K_2^e\right] + \left[K_3^e\right] + \left[K_4^e\right] + \left[K_5^e\right] \tag{4.23}$$

where

$$\left[K_1^e\right] = \frac{G\kappa Al}{2} \begin{bmatrix} 14/3l^2 & -1/l & -16/3l^2 & -4/3l & 2/3l^2 & 1/3l \\ -1/l & 2/9 & 4/3l & 2/9 & -1/3l & -1/9 \\ -16/3l^2 & 4/3l & 32/3l^2 & 0 & -16/3l^2 & -4/3l \\ -4/3l & 2/9 & 0 & 8/9 & 4/3l & 2/9 \\ 2/3l^2 & -1/3l & -16/3l^2 & 4/3l & 14/3l^2 & 1/l \\ 1/3l & -1/9 & -4/3l & 2/9 & 1/l & 2/9 \end{bmatrix}$$

$$\left[K_2^e\right]=\frac{2[EI+(2\mu_0+\lambda_0)I^*]}{l}\begin{bmatrix}0&0&0&0&0&0\\0&7/6&0&-4/3&0&1/6\\0&0&0&0&0&0\\0&-4/3&0&8/3&0&-4/3\\0&0&0&0&0&0\\0&1/6&0&-4/3&0&7/6\end{bmatrix}$$

$$\left[K_3^e\right]=\frac{4\nu I\tau_0}{Hl^2}\begin{bmatrix}0&-1&0&0&0&1\\-1&0&2&0&-1&0\\0&2&0&0&0&-2\\0&0&0&0&0&0\\0&-1&0&0&0&1\\1&0&-2&0&1&0\end{bmatrix}$$

$$\left[K_4^e\right]=\frac{2\tau_0 s^*}{l}\begin{bmatrix}7/6&0&-4/3&0&1/6&0\\0&0&0&0&0&0\\-4/3&0&8/3&0&-4/3&0\\0&0&0&0&0&0\\1/6&0&-4/3&0&7/6&0\\0&0&0&0&0&0\end{bmatrix}$$

$$\left[K_5^e\right]=\frac{F}{2}\begin{bmatrix}0&-1/2&0&-2/3&0&1/6\\-1/2&0&2/3&0&-1/6&0\\0&2/3&0&0&0&-2/3\\-2/3&0&0&0&2/3&0\\0&-1/6&0&2/3&0&1/2\\1/6&0&-2/3&0&1/2&0\end{bmatrix} \tag{4.24}$$

Exact integration is performed to obtain the stiffness matrices $[K_2^e]$, $[K_3^e]$, $[K_4^e]$ and $[K_5^e]$, while reduced-integration technique [57] is used to calculate the shear stiffness term $[K_1^e]$ in order to avoid shear locking [58]. That is, beam elements can have 3 or higher number of nodes. For each case, the shear stiffness matrix needs to be under-integrated consistently. The order of integration for shear stiffness matrix is one less than what is required for exact integration. For example, in the present case the expression of $[K_1^e]$ is a third order polynomial so that the 3-point Gauss quadrature can evaluate the integration exactly. For under-integration, 2-point Gauss quadrature is used to obtain $[K_1^e]$.

For an element subjected to a uniformly distributed load q_0, the force vector can be derived as,

$$\{R^e\} = -\frac{q_0 l}{6}\begin{bmatrix}1 & 0 & 4 & 0 & 1 & 0\end{bmatrix}^T \tag{4.25}$$

4.1.4 Thick Beam Free Vibration

In the dynamic analysis, the consistent element mass matrix can be computed from the inertial forces on the right hand side of equation (4.17) and (4.18).

$$[m] = [m_1^e] + [m_2^e] + [m_3^e] \tag{4.26}$$

where

$$[m_1^e] = \frac{(\rho A + \rho_0 s^*)l}{2}\begin{bmatrix} 4/15 & 0 & 2/15 & 0 & -1/15 & 0 \\ 0 & 0 & 0 & 0 & 0 & 0 \\ 2/15 & 0 & 16/15 & 0 & 2/15 & 0 \\ 0 & 0 & 0 & 0 & 0 & 0 \\ -1/15 & 0 & 2/15 & 0 & 4/15 & 0 \\ 0 & 0 & 0 & 0 & 0 & 0 \end{bmatrix}$$

$$[m_2^e] = \frac{(\rho I + \rho_0 I^*)l}{2}\begin{bmatrix} 0 & 0 & 0 & 0 & 0 & 0 \\ 0 & 4/15 & 0 & 2/15 & 0 & -1/15 \\ 0 & 0 & 0 & 0 & 0 & 0 \\ 0 & 2/15 & 0 & 16/15 & 0 & 2/15 \\ 0 & 0 & 0 & 0 & 0 & 0 \\ 0 & -1/15 & 0 & 2/15 & 0 & 4/15 \end{bmatrix}$$

$$[m_3^e] = \frac{\nu I \rho_0}{2H}\begin{bmatrix} 0 & -1 & 0 & -4/3 & 0 & 1/3 \\ -1 & 0 & 4/3 & 0 & -1/3 & 0 \\ 0 & 4/3 & 0 & 0 & 0 & -8/3 \\ -4/3 & 0 & 0 & 0 & 4/3 & 0 \\ 0 & -1/3 & 0 & 4/3 & 0 & 1 \\ 1/3 & 0 & -8/3 & 0 & 1 & 0 \end{bmatrix}$$

4.2 Finite Element Simulation of Nanoscale Beam Static and Dynamic Response

To assess the accuracy of the proposed finite element formulation, static bending buckling and free vibration problems of selected thin and thick beams are computed and compared with the analytical results obtained from Chapter 2 and 3. The materials used in the simulation are Si and Al, the bulk material properties and surface properties for a [1 0 0] surface of which can be found in Table 2.1. The dimensions for thin beams are $L = 200nm$, $H = 2h = 10nm$ and $b = 10nm$, and those for thick beams are $L = 60nm$, $H = 2h = 10nm$ and $b = 10nm$ in all the calculations.

In the nanoscale beam static analysis, normalized deflections of thin and thick beams under different boundary conditions (simply supported, cantilever and clamped-clamped ends) and loadings (uniformly distributed load q_0 or mid-point load P for SS and CC, tip load P for C) are plotted using FEM and analytical model. It can be seen in Figure 4.3 that the numerical results from the FEM are in good agreement with the analytical solutions, which speaks well of the validity of the new FEM. In each simulation 5 elements are used. As we can see from Figure 4.4, for static deflection the variation is not much once the number of elements reaches certain amount, in this case the results converge very fast after 5 elements.

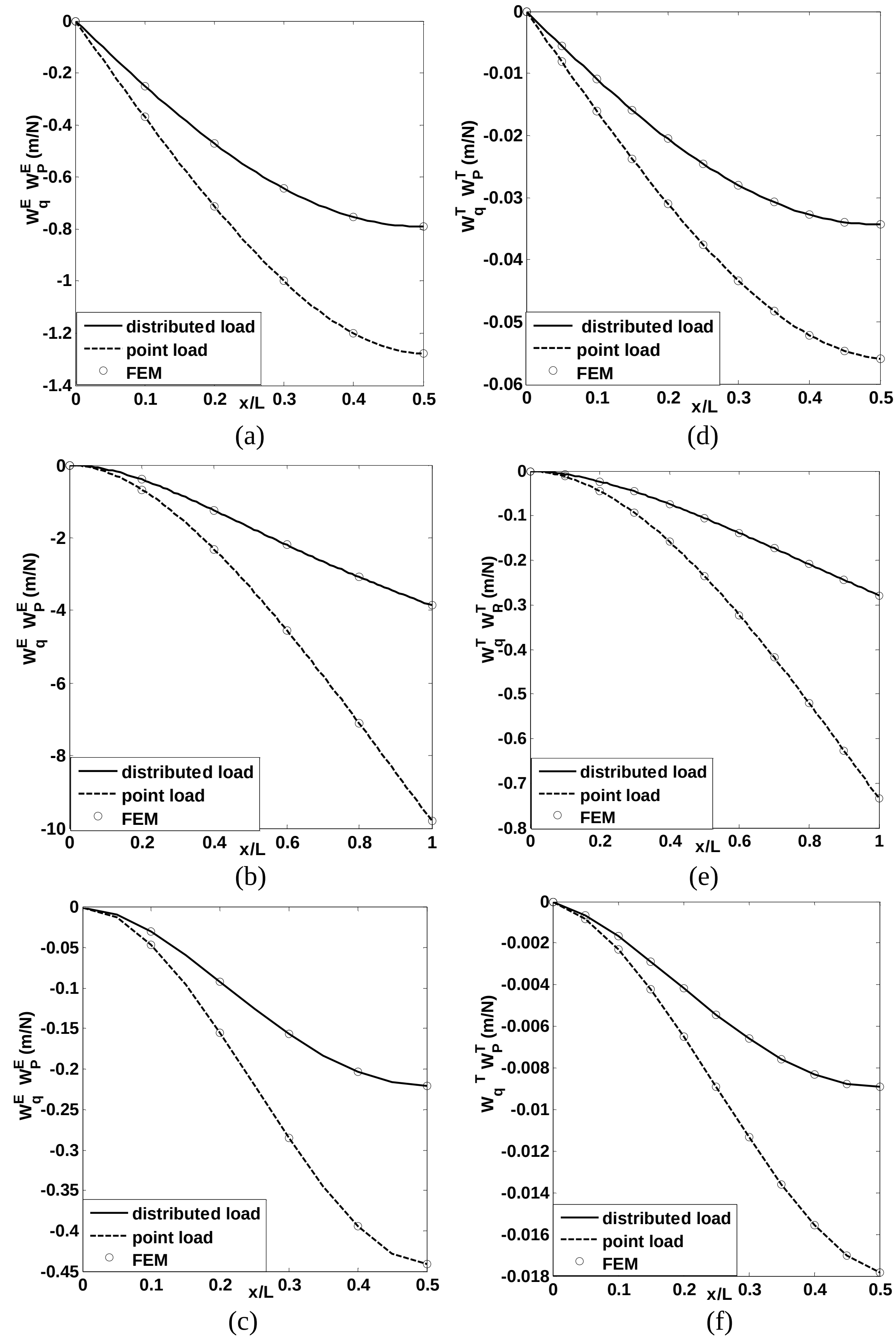

Figure 4.3 Normalized deflections of Si beams under distributed loading and point loading using FEM and analytical model. (a) thin simply supported (b) thin cantilever (c) thin clamped-clamped ends (d) thick simply supported (e) thick cantilever (f) thick clamped-clamped ends

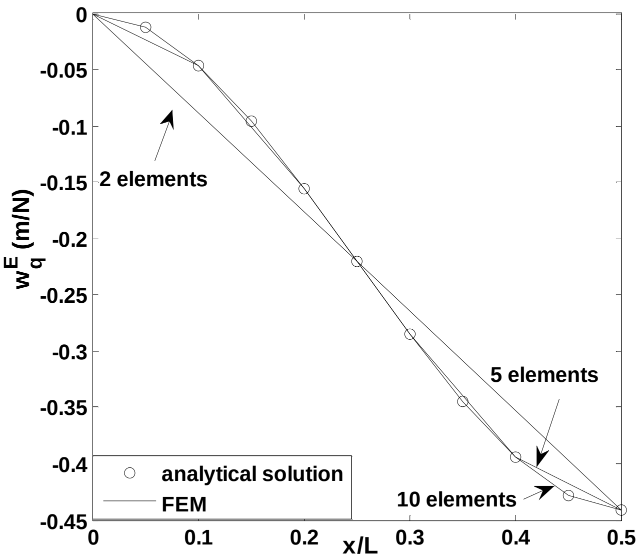

Figure 4.4 Normalized deflections of half Si thin clamped-clamped ends beam under point load P with varied element numbers.

The natural frequencies of beams with above mentioned dimensions are also computed using 20 elements and the first 4 natural frequencies for each case are listed in Table 4.1. The analytical results obtained by solving the characteristic equations of the surface elastic model in Chapter 3 are presented in parenthesis, followed by the results using classical theory in square brackets. The natural frequencies using FEM are slightly higher than the analytical result, which agrees with the principle that FE representation is stiffer than the true continuum. By comparing with the analytical results, the error is within 3%. Such accuracy is adequate for most practical design of NEMS devices. Therefore, we can extend our model to beams with more complicated geometry, loading and boundary conditions confidently. It is found that the mode shapes converge fast after 20 elements. The fourth mode shape of a simply supported beam is plotted using 40 elements as shown in Figure 4.5. The instability of the mode shapes is observed when the element number increases to a high value. A further investigation shows that the reason for the instability is the second term of local mass matrix in equation (4.15) increases dramatically with the decreasing of element length l; therefore, the mass matrix cannot remain positive definite. However, numerical study in Chapter 3 shows that the influence of this term is very small on beam vibrations, therefore it can be neglected in order to avoid the instability in the FE simulations.

Table 4.1 Natural frequencies of Si thin and thick beams under different boundary conditions using FEM, analytical solution are in parenthesis and classical solution in square bracket.

Thin beam	1^{st} (GHz)	2^{nd} (GHz)	3^{rd} (GHz)	4^{th} (GHz)
	0.92 (0.92) [0.77]	3.13(3.13)[3.07]	6.78(6.77)[6.91]	11.90(11.88)[12.29]
	0.45(0.45)[0.27]	1.92(1.92)[1.72]	4.83(4.82)[4.80]	9.19(9.18)[9.40]
	1.77 (1.77)[1.74]	4.72(4.71)[4.80]	9.12(9.10)[9.41]	14.99(14.96)[15.56]
Thick beam				
	8.05(7.96)[8.16]	28.40(28.14)[29.28]	55.87(55.36)[57.30]	86.93(85.94)[89.13]
	3.09(3.09)[2.98]	16.21(16.17)[16.63]	39.68(39.33)[40.74]	67.54(66.85)[69.23]
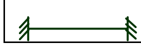	15.88(15.85)[16.42]	37.86(37.60)[38.83]	64.49(64.01)[66.05]	93.69(92.84)[95.49]

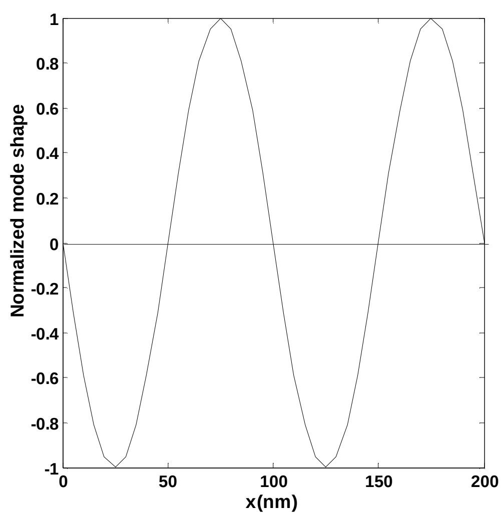

Figure 4.5 Mode shape of a Si simply supported beam using 40 elements

Table 4.2 shows the critical loads of Al and Si beams under aforementioned restrains with dimensions b = 10 nm, 2h = 10 nm and L = 200nm. It can be seen that the critical loads could be changed significantly by the presence of surface effects. The FEM gives a very good prediction compared to the analytical solution.

Table 4.2 Critical loads for beams under different restrains using FEM, analytical solution in parenthesis and classical solution in square bracket.

Beam type	Critical load (nN)	
	Al	Si
	28.67(28.67) [18.51]	32.45(32.45)[22.00]
	15.70 (15.70) [4.63]	17.20(17.20)[5.50]
	80.55(80.53) [74.02]	93.49(93.47)[88.00]

Chapter 5

SUMMARY AND CONCLUSION

5.1 Summary of Present Work and Major Findings

The main purpose of this thesis is to develop a continuum beam model accounting for surface energy effects based on Gurtin-Murdoch elasticity theory to analyze the static and dynamic responses of nanoscale beams. The model is applied specifically to study the static bending, vibration and buckling loads of thick and thin nanoscale beams. Selected numerical results are presented to demonstrate the salient features of the response and to assess the influence of surface energy effects. A new finite element formulation is derived from weighted residual method to analyze complex beam problems. The conclusions of current study are given below.

(1) The governing equations are developed for thin and thick beams with an arbitrary cross-section. Closed-form analytical solutions can be derived for the static deflections of thin and thick beam subjected to uniformly distributed loading and concentrated loads for several common boundary conditions (simply supported, cantilever, both ends clamped). The buckling of nanoscale beams under uniaxial compression is also analyzed and the critical loads under various restraints are derived. The present formulation shows that the surface elastic properties can make the material stiffer or softer than the classical case due to the sign of the surface elastic constants and surface residual stress, and this effect will become more pronounced with the decreasing size. The difference of the results predicted from surface elasticity and classical models relies on the magnitudes of the surface properties. An intrinsic length parameter, controlled by both surface elastic properties and bulk properties can be established to characterize the surface energy effects for beam bending problems. As the height of beam becomes comparable to the intrinsic length, the surface energy effects become important. Selected numerical results show that Al and Si thin beam deflections as well as the critical loads are significantly influenced by surface energy effects. The numerical study demonstrates that large absolute value of negative surface elastic properties at small

dimensions could result in negative K_b (K_s for thick beam), which may consequently lead to deflection instability as well as complex natural frequencies. The reason for this phenomenon is that the non-positive definiteness of surface elastic energy will dominate over the bulk strain energy at small dimensions. In this case, the Gurtin-Murdoch theory essentially breaks down and other atomistic models need to be chosen. Our model is applicable only when the bulk is still the dominant part although the surface contribution is prominent.

(2) The surface energy effects on free vibration of nanoscale beams are investigated and the characteristic equations to determine the natural frequencies are presented. The numerical solutions indicate that the natural frequencies are affected by both surface elastic properties and surface density. The effect of surface residual stress on natural frequencies will decrease with the increase of wave number for higher modes. The impact of surface energy also depends on the beam boundary conditions. The highest influence is observed for cantilever beams followed by simply supported and clamped-clamped beams. Rayleigh quotient is adopted to derive the closed-form analytical solution for natural frequency with surface energy effects. A method to determine the material elastic constants by measuring natural frequencies is thereafter proposed.

(3) A new finite element formulation taking into account surface energy effects has been derived from weighted residual method. It is found that the effect of the surface on the finite element formulation is to change the stiffness and mass matrices of the elements, which consequently change the mechanical behaviour significantly. As a result, the conventional beam theories are inadequate to predict the responses of nanoscale beams. The new finite element scheme is applied to analyze the thin and thick beam static bending and vibration responses as well as thin beam buckling problems; by comparing with the analytical results, the error is within 3%. Such accuracy is adequate for most practical design of NEMS devices. The FEM model developed in this thesis provide an efficient tool for NEMS designers to investigate the component structures in device design.

5.2 Suggestions for Future Work

Based on the findings of the thesis, it is recommended that the following studies be undertaken to further understand the mechanics of nanoscale structures;

(1) In the present work, the beam models are built based on the classical assumption of small strains and small displacements. This is sufficient to analyze static and dynamic behavior of a beam within small deflections. In many practical cases, the structures can undergo large scale elastic deflection; therefore it is useful to examine the surface energy effects on large-deflection (elastica) based problems.

(2) Finite element study is conducted to study the static and dynamic response of nanoscale beams. The transient analysis is also suggested to be implemented into the current finite element scheme.

(3) The thesis proposed an energy method based on Rayleigh quotient to predict the natural frequency of beam and the material properties, provided that an appropriate trial function is adopted to approximate the beam true mode shape. The selection of the trial function needs to be further investigated in order to obtain accurate solution.

(4) Current study shows that the static and dynamic response of nanoscale beams are significantly dependent on the surface elastic properties. Therefore, precise measurement technique or efficient atomistic computational means are required to extract those properties. Meanwhile, experimental studies and atomistic simulations are also recommended for validation and further extension of our surface elastic model and finite element scheme presented in this work.

(5) The beam theories developed in this work are based on simplified state of stress of the three-dimensional elastic solid. In the spirit of engineering beam theory we introduced surface elasticity effects. It is also possible to solve the complete three-dimensional elasticity problem using appropriate stress functions. This may provide an alternate route to validate the modified engineering beam theories proposed in this work.

(6) In classical elasticity and beam theories we invoke Saint Venant's principle to study the influence of boundaries, or sudden changes in cross section. The scaling of Saint Venant elastic boundary layer thickness in small scale system remains an open problem.

BIBLIOGRAPHY

[1] Feynman, R.P., 1960, "There's Plenty of Room at the Bottom: An Invitation to Enter a New Field of Physics," Engineering and Science, **23**(5), pp. 22–36.

[2] Lourie, O. and Wagner, H.D., 1998, "Evaluation of Young's Modulus of Carbon Nanotubes by Micro-Raman Spectroscopy," Journal of Materials Research, **13(9),** pp. 2418-2422.

[3] Peng, B., Locascio, M. and Zapol, P., 2008, "Measurements of Near-Ultimate Strength for Multiwalled Carbon Nanotubes and Irradiation-Induced Crosslinking Improvements," Nature Nanotechnology, **3**(10), pp. 626-631.

[4] Roco, M.C., Williams, R.S., and Alivisatos, P., 2000, "Nanotechnology research directions," Kluwer academic publishers, Netherlands.

[5] Tomasetti, E., Nysten, B., and Legras, R., 1998, "Quantitative Approach towards the Measurement of Polypropylene/ (Ethylene-Propylene) Copolymer Blends Surface Elastic Properties by AFM**,**" Nanotechnology, **9,** pp. 305-315.

[6] Cuenot, S., Frétigny, C., Demoustier-Champagne, S., 2004, "Surface Tension Effect on the Mechanical Properties of Nanomaterials Measured by Atomic Force Microscopy," Physical Review B, **69**(165), pp. 410-411.

[7] Wong, E. W., Sheehan, P. E., and Lieber, C. M., 1997, "Nanobeam Mechanics: Elasticity, Strength and Toughness of Nanorods and Nanotubes," Science, **277**(5334), pp. 1971.

[8] Han, X. D., Zhang, Y. F., and Zheng, K. and Zhang, Z., 2007, "Direct Observation of Low-Temperature Large Strain Plasticity and Atomic Mechanisms of Ceramic SiC Nanowires," Nano Letters, **7,** pp. 452.

[9] Ohno, K., Esfarjani, K., and Kawazoe, Y., 1999, "Computational Material Science: From Ab Initio to Monte Carlo Method," Springer, Berlin, Germany.

[10] Streitz, F. H., Cammarata, R. C., and Sieradzki, K., 1994, "Surface-Stress Effects on Elastic Properties. I. Thin Metal Films," Physical Review B, **49(15),** pp. 10699-10706.

[11] Gibbs, J. W., 1906, "The Scientific Papers of J. Willard Gibbs," Dover Publications, Inc, New York.

[12] Yakobson, B. I., 2003, "Nanomechanics, Handbook of Nanoscience, Engineering and Techology," CRC Press, Boca Raton.

[13] Shuttleworth, R., 1950, "The Surface Tension of Solids," Proceedings of the Physical Society Section A, **63**(5), pp. 444-457.

[14] Cammarata, R. C., 1994, "Surface and Interface Stress Effects in Thin Films," Progress in Surface Science, **46**(1), pp. 1-38.

[15] Nix, W. D., and Gao, H., 1998, "An Atomistic Interpretation of Interface Stress," Scripta Materialia, **39**(12), pp. 1653-1661.

[16] Miller, R. E. and Shenoy, V. B., 2000, "Size-Dependent Elastic Properties of Nanosized Structural Elements," Nanotechnology, **11**(3), pp. 139-147.

[17] Shenoy, V. B., 2005, "Atomistic Calculations of Elastic Properties of Metallic Fcc Crystal Surfaces," Physical Review B, **71**(9), pp. 094104.

[18] Gurtin, M. E. and Murdoch, A. I., 1975, "A Continuum Theory of Elastic Material Surfaces," Archive for Rational Mechanics and Analysis, **57**(4), pp. 291-323.

[19] Gurtin, M. E. and Murdoch, A. I., 1978, "Surface Stress in Solids," International Journal of Solids and Structures, **14**(6), pp. 431–440.

[20] Vermaak, J. S., Mays, C. W. and Kuhlmann-Wilsdorf, D., 1968, "On Surface Stress and Surface Tension: I. Theoretical Considerations," Surface Science, **12**(2), pp. 128-133.

[21] Wasserman, H. J. and Vermaak, J. S., 1972, "On the Determination of the Surface Stress of Copper and Platinum," Surface Science, **32**(1), pp. 168-174.

[22] Jing, G. Y., Duan, H. L. and Sun, X. M., 2006, "Surface Effects on Elastic Properties of Silver Nanowires: Contact Atomic-Force Microscopy," Physical Review B, **73**(23), pp, 235409.

[23] Ibach, H., 1999, "Erratum to:The Role of Surface Stress in Reconstructin, Epitaxial Growth and Stabilization of Mesoscopic Structure," Surface Science Reports, **35,** pp. 71.

[24] Ibach, H., 1997, "The Role of Surface Stress in Reconstructin, Epitaxial Growth and Stabilization of Mesoscopic Structure," Surface Science Reports, **29,** pp. 193-246.

[25] Maede, R. D. and Vanderbilt, D., 1989, "Origins of Stress on Elemental and Chemisorbed Semiconductor Surfaces," Physical Review Letters, **63**(13), pp. 1404-1407.

[26] Needs, R. J., 1987, "Calculations of the Surface Stress Tensor at Aluminum (111) and (110) Surfaces," Physical Review Letters, **58**(1)pp. 53-56.

[27] Dingreville, R., and Qu, J., 2007, "A Semi-Analytical Method to Compute Surface Elastic Properties," Acta Materialia, **55**(1)pp. 141-147.

[28] Dingreville, R., Kulkarni, A. J. and Zhou, M., 2008, "A Semi-Analytical Method for Quantifying the Size-Dependent Elasticity of Nanostructures," Modelling and Simulation in Materials Science and Engineering, **16**(2)pp. 25002.

[29] Hamilton, J. C., and Wolfer, W. G., 2009, "Theories of Surface Elasticity for Nanoscale Objects," Surface Science, **603**pp. 1284-1291.

[30] Shenoy, V. B., 2002, "Size-Dependent Rigidities of Nanosized Torsional Elements," International Journal of Solids and Structures, **39**(15)pp. 4039-4052.

[31] Wang, Z. Q., Zhao, Y. P., and Huang, Z. P., 2009, "The Effects of Surface Tension on the Elastic Properties of Nano Structures," International Journal of Engineering Science, **in press**.

[32] Sharma, P., Ganti, S., and Bhate, N., 2003, "Effect of Surfaces on the Size-Dependent Elastic State of Nano-Inhomogeneities," Applied Physics Letters, **82** pp. 535.

[33] Sharma, P., and Wheeler, L. T., 2007, "Size-Dependent Elastic State of Ellipsoidal Nano-Inclusions Incorporating Surface⁄ Interface Tension," Journal of Applied Mechanics - Transactions of the ASME, **74**(3)pp. 447-454.

[34] Tian, L., and Rajapakse, R. K. N. D., 2007, "Elastic Field of an Isotropic Matrix with a Nanoscale Elliptical Inhomogeneity," International Journal of Solids and Structures, **44**(24)pp. 7988-8005.

[35] Wang, G. F., and Feng, X. Q., 2007, "Effects of Surface Stresses on Contact Problems at Nanoscale," Journal of Applied Physics, **101**pp. 013510.

[36] Zhao, X. J., and Rajapakse, R. K. N. D., 2009, "Analytical Solutions for a Surface-Loaded Isotropic Elastic Layer with Surface Energy Effects," International Journal of Engineering Science, **in press**.

[37] Craighead, H. G., 2000, "Nanoelectromechanical Systems," Science, **290**pp. 1532-1535.

[38] Lagowski, J., Gatos, H. C., and Sproles Jr., E. S., 1975, "Surface Stress and Normal Mode of Vibration of Thin Crystal: GaAs," Applied Physics Letters, **26**pp. 493.

[39] Gurtin, M. E., Markenscoff, X., and Thurston, R. N., 1976, "Effect of Surface Stress on the Natural Frequency of Thin Crystals," Applied Physics Letters, **29**pp. 529.

[40] Wang, G. F. and Feng, X. Q., 2007, "Effects of Surface Elasticity and Residual Surface Tension on the Natural Frequency of Microbeams," Applied Physics Letters, **90** pp. 231904.

[41] Yang, Y. T., Ekinci, K. L. and Huang, M. H., 2001, "Monocrystalline Silicon Carbide Nanoelectromechanical Systems," Applied Physics Letters, **78**pp. 162-164.

[42] Ekinci, K. L. and Roukes, M. L., 2005, "Nanoelectromechanical Systems," Review of Scientific Instruments, **76**pp. 061101.

[43] Wang, G. F., Feng, X. Q., and Yu, S. W., 2007, "Surface Buckling of a Bending Microbeam due to Surface Elasticity," Europhysics Letters, **77**pp. 44002.

[44] Sadeghian, H., Yang, C. K., Gavan, K. B., Goosen, J. F. L., van der Drift, E. W. J. M., van der Zant, H. S. J., French, P. J., Bossche A. and van Keulen, F., 2009, "Effects of Surface Stress on Nanocantilevers," Surface Science and Nanotechnology, **7**pp. 161-166.

[45] Lachut, M. J., and Sader, J. E., 2007, "Effect of Surface Stress on the Stiffness of Cantilever Plates," Physical Review Letters, **99**pp. 206102.

[46] Lim, C. W., and He, L. H., 2004, "Size-Dependent Nonlinear Response of Thin Elastic Films with Nano-Scale Thickness," International Journal of Mechanical Sciences, **46**(11) pp. 1715-1726.

[47] Lu, P., He, L. H., Lee, H. P., 2006, "Thin Plate Theory Including Surface Effects," International Journal of Solids and Structures, **43**(16) pp. 4631-4647.

[48] He, L. H., Lim, C. W. and Wu, B. S., 2004, "A Continuum Model for Size-Dependent Deformation of Elastic Films of Nano-Scale Thickness," International Journal of Solids and Structures, **41**(3-4) pp. 847-857.

[49] He, J. and Lilley, C. M., 2008, "Surface Effect on the Elastic Behavior of Static Bending Nanowires," Nano Letters, **8**(7) pp. 1798-1802.

[50] He, J., and Lilley, C. M., 2008, "Surface Stress Effect on Bending Resonance of Nanowires with Different Boundary Conditions," Applied Physics Letters, **93**pp. 263108.

[51] Gere J. M. and Timoshenko, S. P., 1995, "Mechanics of Materials," Chapman and Hall Ltd., London, England.

[52] Timoshenko, S. P., 1932, "Schwingungsprobleme der technik," Verlag von Julius, Springer, Berlin, Germany.

[53] Zhu, H. S., Wang, J. X. and Karihaloo, B., 2009, " Effects of Surface and Initial Stresses on the Bending Stiffness of Trilayer Plates and Nanofilms", Journal of Mechanics of Materials and Structures, **4**pp. 589-604.

[54] Daw, M. S. and Bakes, M. I., 1984, "Embedded-Atom Method: Derivation and Application to Impurities, Surfaces, and Other Defects in Metals," Physics Review B, **29**pp. 6443-6453.

[55] Huang, T. C., 1961, "The Effect of Rotary Inertia and of Shear Deformation on the Frequency and Normal Mode Equations of Uniform Beams with Simple End Conditions." American Society of Mechanical Engineers, Journal of Applied Mechanics, **28**pp. 579-584.

[56] Washizu, K., 1962, "Variational Principles in Continuum Mechanics," Department of Aeronautical Engineering Report, 62-2, University of Washington, Seattle, WA.

[57] Zienkiewicz, O. C., Taylor, R. L., and Too, J. M., 1971, "Reduced Integration Technique in General Analysis of Plates and Shells," International Journal for Numerical Methods in Engineering, **3**pp. 275-290.

[58] Kwon, Y.W., and Bang, H., 1997, "The Finite Element Method Using Matlab", CRC Press, pp. 244.